

## Durham Research Online

---

### Deposited in DRO:

31 May 2018

### Version of attached file:

Accepted Version

### Peer-review status of attached file:

Peer-reviewed

### Citation for published item:

Sossi, P. A. and Prytulak, J. and O'Neill, H. St. C. (2018) 'Experimental calibration of vanadium partitioning and stable isotope fractionation between hydrous granitic melt and magnetite at 800C and 0.5GPa.', Contributions to mineralogy and petrology., 173 (4). p. 27.

### Further information on publisher's website:

<https://doi.org/10.1007/s00410-018-1451-8>

### Publisher's copyright statement:

The final publication is available at Springer via <https://doi.org/10.1007/s00410-018-1451-8>.

### Additional information:

---

### Use policy

The full-text may be used and/or reproduced, and given to third parties in any format or medium, without prior permission or charge, for personal research or study, educational, or not-for-profit purposes provided that:

- a full bibliographic reference is made to the original source
- a [link](#) is made to the metadata record in DRO
- the full-text is not changed in any way

The full-text must not be sold in any format or medium without the formal permission of the copyright holders.

Please consult the [full DRO policy](#) for further details.

# Experimental calibration of vanadium partitioning and stable isotope fractionation between hydrous granitic melt and magnetite at 800°C and 0.5 GPa

Paolo A. Sossi<sup>1\*</sup>, Julie Prytulak<sup>2</sup> & Hugh St.C. O'Neill<sup>1</sup>

<sup>1</sup> Research School of Earth Sciences, Australian National University, Canberra, 2601, ACT, Australia

<sup>2</sup> Department of Earth Science and Engineering, Imperial College London, SW7 2AZ, UK

\*Corresponding author. Present address: Institut de Physique du Globe de Paris, Sorbonne Paris Cité, Université Paris Diderot, CNRS, F-75005 Paris, France. *E-mail address*: sossi@ipgp.fr

## Abstract

Vanadium has multiple oxidation states in silicate melts and minerals, a property that also promotes fractionation of its isotopes. As a result, vanadium isotopes vary during magmatic differentiation, and can be powerful indicators of redox processes at high temperatures if their partitioning behaviour can be determined. In order to quantify the isotope fractionation factor between magnetite and melt, piston cylinder experiments were performed in which magnetite and a hydrous, haplogranitic melt were equilibrated at 800°C and 0.5 GPa over a range of oxygen fugacities ( $fO_2$ ), bracketing those of terrestrial magmas. Magnetite is systematically  $^{51}\text{V}$ -depleted with respect to the coexisting melt, a tendency ascribed to the predominantly VI-fold  $\text{V}^{3+}$  in magnetite, and a mixture of IV- and VI-fold  $\text{V}^{5+}$  and  $\text{V}^{4+}$  in the melt. The magnitude of the fractionation factor systematically increases with increasing  $\log fO_2$  relative to the Fayalite-Magnetite-Quartz buffer (FMQ), from  $\Delta^{51}\text{V}_{\text{mag-gl}} = -0.63 \pm 0.09\text{‰}$  at FMQ-1 to  $-0.92 \pm 0.11\text{‰}$  (SD) at  $\approx \text{FMQ}+5$ . These first mineral-melt measurements of V isotope fractionation factors underline the importance of both oxidation state and co-ordination environment in controlling isotopic fractionation. The fractionation factors determined experimentally are in excellent agreement with those needed to explain natural isotope variations in magmatic suites. Further, these experiments provide a useful framework in which to interpret vanadium isotope variations in natural rocks and magnetites, and may be used as a potential fingerprint the redox state of the magma from which they crystallise.

Keywords: Redox, Magnetite, Magma, Vanadium, Stable Isotope Fractionation, Equilibrium

Word Count = 7,287; Figures = 6; Tables = 8

## Introduction

Among the polyvalent elements, vanadium is particularly unique in that it exists in five oxidation states,  $V^0$ ,  $V^{2+}$ ,  $V^{3+}$ ,  $V^{4+}$  and  $V^{5+}$ . This wide range of valence states brackets the oxygen fugacities ( $fO_2$ ) of natural rocks, and thus elemental partitioning of V has been employed as a redox indicator (e.g., Canil 1997; Lee et al. 2005; Mallmann and O'Neill, 2009; 2013).

Pure magnetite has an inverse spinel structure at room temperature, with the formula  $^{IV}(Fe^{3+})^{VI}(Fe^{2+}Fe^{3+})O_4$ , however, it tends to the random, normal distribution at  $\approx 1400^\circ C$  (Wu and Mason, 1981). In the absence of titanium, the  $Fe^{3+}/Fe^{2+}$  ratio of two in magnetite is imposed by its stoichiometry, making it independent of  $fO_2$  of the melt from which it crystallises. The high octahedral site preference energy of  $V^{3+}$  makes its incorporation favourable into magnetite by the reaction  $VO_{1.5} + FeO = FeV_2O_4$ , which is a normal spinel. Together, the  $Fe^{3+}/Fe^{2+}$  and  $V^{4+}/V^{3+}$  pairs undergo electron exchange that results in the stabilisation of all four species at high temperatures, leading to considerable configurational entropy and negative deviations from ideality in  $Fe_3O_4$ - $FeV_2O_4$  solid solutions (Petric and Jacob, 1982; O'Neill and Navrotsky, 1984). This phenomenon renders  $V^{3+}$  highly compatible in magnetite, and the  $V^{4+}/V^{3+}$  ratio is also independent of  $fO_2$  at a given temperature and pressure.

Due to the important role magnetite plays in evolving magmas, vanadium partition coefficients are well-characterised over a range of  $fO_2$  (e.g., Canil and Fedourtchuk, 2001; Richter et al., 2006a; Toplis and Corgne, 2002, Mallmann & O'Neill, 2009), though, until recently, few at melt compositions relevant to the silicic magmas from which they predominantly crystallise. Arató and Audétat (2017) measured the partitioning of V between magnetite and silicic melts with varying Alumina-Saturation Indices (ASI), molar  $Al_2O_3/(CaO+Na_2O+K_2O)$ , between  $800^\circ C$  and  $1000^\circ C$ , observing that V becomes more compatible at lower temperatures and higher ASI. A similar dependence was observed by Sievwright et al. (2017), who further showed that V substitution into titanomagnetite follows that of Ti. In both cases, the logarithm of the partition coefficient of V into magnetite compared with  $\log fO_2$  resulted in a slope of -0.5, implying that V is largely trivalent in magnetite, whereas  $V^{5+}$  prevails in the silicate liquid.

Stable V isotopes can now be determined to a precision high enough to be applied to geological problems (e.g., Nielsen et al., 2011; Prytulak et al., 2011; Wu et al., 2016). The nascent dataset, including peridotites, mafic magmas and meteorites (Prytulak et al., 2011; Prytulak et al. 2013, Nielsen et al. 2014; Wu et al., 2016; Prytulak et al. 2017; Schuth et al. 2017; Sossi et al. 2017) reveals analytically resolvable V isotope fractionations at high temperatures. The strong dependence of V partitioning on  $fO_2$  makes it tempting to interpret isotope variations in terms of variable oxygen fugacity. Even at igneous temperatures, variable bond strength gives rise to stable isotope

fractionation, with heavier isotopes preferred in stronger bonding environments (e.g. Urey, 1947; Schauble, 2004). Whilst the valence of an element plays a role in determining bond strength, the co-ordination environment is also key (e.g., Sossi and O'Neill, 2017).

Vanadium isotopes, during the early phase of crystallisation dominated by Fe-Mg silicates and plagioclase, are invariant in natural magmatic systems from island arc (Marianas) and intraplate (Hekla, Iceland) environments (Prytulak et al., 2017), and V is mildly incompatible. However, upon Fe-Ti oxide saturation in dacitic compositions, the V isotope composition of the remaining melt increases to 2‰ higher than in mafic compositions. This phenomenon is a result of Rayleigh distillation and a magnetite-melt fractionation factor of  $\approx -0.5\%$  at around 1000-1050°C (Prytulak et al., 2017). At the resolution of their measurements, no co-variation of the fractionation factor with the  $fO_2$  of the magma (FMQ for Hekla, FMQ+2 for Marianas) is apparent. As such, both the differing co-ordination and V oxidation state inferred between magnetite ( $^{VI}V^{3+}$ ) and melt ( $^{IV-VI}V^{4+}$  and  $^{IV}V^{5+}$ ) are required to drive isotopic fractionation, but it is problematic to deconvolve these parameters from one another in natural rocks. Thus, before natural variations in stable vanadium isotopes can be interpreted in the context of  $fO_2$ , the response of isotope fractionation to oxygen fugacity and other physicochemical variables must be systematically examined.

This contribution presents the first experimental investigation of stable vanadium isotope fractionation. Stable V isotope fractionation factors are determined between hydrous, granitic melts and magnetite equilibrated in a piston cylinder assembly at 800°C and 0.5 GPa as a function of oxygen fugacity. These conditions were chosen to maximise the isotopic fractionation factor whilst still resembling natural systems. Elemental partitioning between the two phases is fit using a thermodynamic model that yields estimates for  $Fe^{2+}/Fe^{3+}$  and  $V^{3+}/V^{4+}/V^{5+}$  ratios in the melt. With this information, V isotope fractionation between magnetite and melt is modelled using the bond valence model. It is shown that V isotope fractionation between experimental magnetite and melt is sensitive to both co-ordination environment and oxygen fugacity, and thus potentially useful in deciphering redox conditions during igneous processes and for fingerprinting the origin of magnetite with differing petrogenetic histories.

## Methods & Rationale

### Experimental Petrology

Magnetite has several attributes that make it an attractive target for the experimental investigation of vanadium stable isotope fractionation. These include the ubiquity of magnetite in igneous systems, the importance of the mineral in understanding the genesis of arc magmas (e.g., Jenner et al., 2010), the high compatibility of vanadium in magnetite (except under very oxidising conditions; Toplis and

Corgne, 2002), the growing body of work using magnetite chemistry for economic tracing (e.g., Boutroy et al. 2014; Dare et al. 2014; Canil et al. 2016) and its magnetic properties, which aids phase separation of experimental charges. Importantly, incorporation of  $V^{3+}$  in magnetite is favoured stoichiometrically over other oxidation states, so that its speciation is independent of oxygen fugacity (O'Neill and Navrotsky, 1984) hence isotopic variations can be ascribed almost solely to changes in V bonding environment in the melt.

Whilst analytically resolvable variations in vanadium isotopes have been demonstrated in high temperature materials (Prytulak et al., 2011; 2013; Nielsen et al., 2014; Prytulak et al. 2017; Schuth et al. 2017; Sossi et al. 2017), the magnitude of fractionation is  $\approx 1\%$ . Thus, the experiments presented herein were devised to maximise potential isotope fractionation, rather than replicate natural systems. Temperature affects stable isotope fractionation proportional to  $1/T^2$  (Urey, 1947). In attempting to minimise temperatures (and therefore maximise isotope fractionation) required for a liquid melt to exist, a haplogranitic melt was chosen (Table 1). To further decrease the liquidus temperature and promote equilibration, water was added as a flux. By interpolation of  $H_2O$  contents at saturation in different haplogranite compositions (Holtz et al., 2001), water saturation is calculated to be 10.2 wt. % at 800°C and 0.5 GPa for the haplogranite used in this work (Table 1). In order to prevent the formation of a fluid phase, which could complex V, 9 wt. % water was added, keeping the melt just below the saturation point. Vanadium was added at 4 wt. % of the total mixture.

In order to control  $fO_2$  in piston cylinder experiments, the double capsule method (Eugster, 1957; Woodland and O'Neill, 1997; Matjuschkin et al., 2015) was employed. This technique is predicated on the rapid diffusion of hydrogen and use of  $H_2O$  as an oxygen buffering agent, where the  $\frac{f_{O_2}}{f_{H_2}}$  ratio is controlled by the redox potential of the  $E^0/E^{x+}$  pair. More reducing metals will be in equilibrium with a vapour phase that has a lower  $H_2O/H_2$  ratio.



Then, subtracting equation (2) from (1) gives:



Hydrogen diffusion proceeds from the outer reservoir into the inner capsule, which is fashioned from a 0.2 mm wall thickness, 3.5 mm external diameter  $Ag_{75}Pd_{25}$ , rather than the pure Ag, 6.3 mm external diameter outer capsule. The Silver-Palladium capsule is less prone to Fe loss compared to Pt (Muan, 1963), and offers comparable  $H_2$  permeability that is an order of magnitude greater than that of pure silver at 800°C (Chou, 1986). At equilibrium, equation (3) can be expressed as:

$$\log f_{O_2} = 2 \log a_{H_2O} - 2 \log f_{H_2} + 2 \log K . \quad (4)$$

If the hydrogen pressures are equivalent in the inner and outer capsules,  $f_{O_2}$  should be equivalent in both. However, in the experiments designed here,  $H_2O$  is slightly undersaturated in the inner capsule, yielding an  $a_{H_2O} < 1$ . Therefore, the oxygen fugacity in the inner capsule is given by:

$$\log f_{O_2}^{inner} = \log f_{O_2}^{outer} + 2 \log a_{H_2O} . \quad (5)$$

Here, it is assumed that the activity of water,  $a_{H_2O} = f_{H_2O}/f_{H_2O}^o$ , where  $f^o$  is the fugacity at saturation (= 1). Mole fractions of water dissolved in granitic melts were calculated as a function of composition at 800°C according to Behrens and Jantos (2000).

The solid-solid buffers chosen span the range of typical terrestrial oxygen fugacities found in granitic rocks (*e.g.*, Carmichael, 1991). At 800°C, they become more oxidising from Co-CoO < NNO < Re-ReO<sub>2</sub> < HM, corresponding to FMQ-0.78, FMQ+0.81, FMQ+2.87 and FMQ+5.07, respectively. As the intrinsic  $f_{O_2}$  of piston cylinder charges are around FMQ (Boettcher et al., 1973; Medard et al., 2008), the molar ratios of the metal-metal oxide mixtures were set such that the more unstable component was in excess. For Co:CoO, 75:25, Ni:NiO = 50:50, Re:ReO<sub>2</sub> = 67:33 and 75:25 Hematite:Magnetite. The presence of water and both phases was verified after the experiment by XRD, ensuring that the oxygen fugacity was buffered by the two-phase assemblage, to an uncertainty of  $\pm 0.3$  log units (Matjuschkin et al., 2015).

To verify the reliability of the more complex piston cylinder experiments, a simpler experiment was run in a 1 atm vertical gas-mixing furnace. A sodium silicate melt composition in the system Na<sub>2</sub>O-SiO<sub>2</sub>-Fe<sub>2</sub>O<sub>3</sub> was devised (Bowen et al., 1930) to remain super-solidus at 800°C and fluid-absent conditions. The oxides were added in the proportions 23:37:38 (Table 1), yielding a composition with a liquidus temperature around 900°C. Above the hematite-magnetite buffer, liquids of this composition crystallise only hematite down to the ternary eutectic temperature of 809°C. To this mix, 2 wt. % V<sub>2</sub>O<sub>3</sub> was added, and the experiment was run in an open Ag crucible suspended from an alumina loop by Pt wire at FMQ-1. Oxygen fugacity was set by a CO-CO<sub>2</sub> gas mixture, with which the melt interacted at 800°C to crystallise magnetite. A summary of experimental conditions, run times and weights can be found in Table 2.

The experiments were finely crushed, and magnetite was separated gravitationally by settling in acetone, where the recovered material was subjected to the same treatment several times, resulting in near-pure glass fractions. Experiments with coarser-grained magnetite were also separated magnetically from the silicate glass. The sodium silicate composition has the added benefit of being soluble in water (Fuchs, 1825), whereas magnetite was dissolved in 6M HCl.

## Electron Microprobe

Major element analyses of the experimentally-grown phases were performed on a Cameca SX100 at the Research School of Earth Sciences (RSES), Australian National University (RSES, ANU) using wavelength dispersive spectroscopy (WDS). Spectrometers were initially calibrated for peak position and intensity on in-house natural mineral standards, and three Smithsonian National History Museum internal standards, San Carlos Olivine, Kakanui Augite and Tiebaghi Chromite (Jarosewich et al., 1980) corrected for in-run drift. Beam conditions were set at 15 kV and 20 nA for a 1 µm focused spot, increased to 20 µm broad beam for glasses. Peak counting times varied depending on the element; Si, Al and Mg were run on TAP with a 10 s count time each while Na was analysed for 20s on the same crystal. Calcium and K were run on PET for 10 s and 20 s, respectively. Iron was analysed for 10 s on the more sensitive LLIF crystal, together with the V K $\alpha$  peak (as opposed to K $\beta$  which is less intense and has interferences from Cr and especially Ti) with a count time of 120 s on two spectrometers, yielding an estimated detection limit of 40 ppm. Reported glass and mineral compositions are an average of between 5 – 10 points.

## Isotope Geochemistry

### *Analytical Considerations*

Vanadium has two stable isotopes, whose abundances are highly skewed between  $^{51}\text{V}$  (99.76%) and  $^{50}\text{V}$  (0.24%). The existence of only two stable isotopes precludes the use of a double spiking technique to correct for mass fractionation. Mass fractionation of stable isotopes may be induced during ion exchange chromatography due to incomplete elution (see Anbar et al., 2000; Chapman et al., 2006; Sossi et al., 2015). Therefore, quantitative (100%) recovery of V is required. In addition, the purification of V is further complicated by the isobaric interferences of  $^{50}\text{Cr}$  and  $^{50}\text{Ti}$  (4.31% and 5.34%, respectively) on the minor isotope,  $^{50}\text{V}$ . As such, the accurate and precise measurement of the isotopes of vanadium also necessitates near-quantitative removal of Cr and Ti (Nielsen et al., 2011; Prytulak et al., 2011).

### *Ion Exchange Chromatography*

Samples, including separated experimental charges and United States Geological Survey (USGS) reference materials were dissolved in HCl-HF-HNO<sub>3</sub> in the ratio 1:0.5:0.2 for 48 hours at 140°C in sealed Teflon vials. The USGS reference material PCC-1 is a Cr-spinel rich harzburgite, that was digested in an oven in pressurised, sealed Teflon bombs in a 3:1 mixture of concentrated HNO<sub>3</sub>:HF for 6 days at 210°C. PCC-1 was then evaporated under concentrated HNO<sub>3</sub>.

The procedure of Nielsen et al. (2011) was followed in order to satisfy the requirements of 1) complete recovery of V and 2) quantitative removal of Cr and Ti. All work was carried out in a laminar flow hood at RSES, ANU.

## Mass Spectrometry

Analyses were performed on a ThermoFinnigan Neptune Plus MC-ICP-MS at RSES, ANU. Stable vanadium isotopes are reported using standard delta notation, relative to the Oxford Alfa Aesar V solution standard (AA), defined as 0‰ (Nielsen et al., 2011; Prytulak et al., 2011).

$$\delta^{51}V_{AA} (\text{‰}) = \left( \frac{(^{51}V/^{50}V)_{\text{mp}}}{(^{51}V/^{50}V)_{AA}} - 1 \right) \times 1000 \quad (6)$$

The Neptune Plus at ANU is equipped with  $10^{10} \Omega$  and  $10^{11} \Omega$  resistors. The major isotope,  $^{51}\text{V}$  was measured on a  $10^{10}$  resistor to mute the overwhelming signal whilst still achieving statistically meaningful counts on  $^{50}\text{V}$ . The measurement protocol followed that outlined in Sossi et al. (2017). Briefly, sample solutions and standards were analysed in 0.3M  $\text{HNO}_3$  at a concentration of 4 ppm, in Low Resolution (LR) mode, using H-cones. Each analysis comprised of 45 cycles of 4.194 s each. An instrumental baseline is implemented before each analysis, in addition to a blank subtraction performed every bracketing standard. The cup configuration is given in Table 3, and allows for collection of the Ti and Cr masses, a requirement for application of the interference correction on  $^{50}\text{V}$ . Interference and mass bias corrections were applied using the exponential law to both the samples and standard. Uncertainties are reported as standard deviations throughout.

## Results

### Petrography

A back-scattered electron image of a representative section of the Re-ReO<sub>2</sub> experiment is shown in Figure 1. All experimental runs produced magnetite and glass. The two phases are present in 1:1 proportions, reflecting the ratio of magnetite:haplogranite in the starting mixture (Table 1). Magnetite predominantly occurs as small (5-20  $\mu\text{m}$ ) euhedral crystals that often form glomeroporphyritic clusters of  $\approx 100\mu\text{m}$ . A small fraction (5-10%) of the magnetite occurs as larger, embayed phenocrysts of up to 50  $\mu\text{m}$  in length, whose growth may have resulted from pressure fluctuations over the course of the experiments. The glass is vitric and unvesiculated. Both magnetite and glass phases are homogeneous, with no chemical zoning evident with proximity to the capsule walls, within phases or where both are in contact.

### Major and Minor element compositions

Compositions of silicate glass and magnetite are reported in Table 4. Water contents, calculated by difference of the total to 100 wt. %, range from 6.89 wt. % (HM) to 9.45 wt. % (NNO), likely reflecting the imprecision in adding 9 $\mu\text{L}$  of water to the experimental charge. Importantly, these are all lower than the theoretical water saturation content of the granitic melt (Holtz et al., 2001). With



respect to the initial starting composition, the alkali contents are depleted, ranging from a combined total of 6.25 to 6.79 wt. % on an anhydrous basis, compared to 9.48 wt. % in the starting mix. Their decrease is at the expense of  $\text{Al}_2\text{O}_3$ ,  $\text{FeO}^{(\text{T})}$  and  $\text{V}_2\text{O}_3$ , with the latter two showing trends in their concentration with  $f\text{O}_2$  (Fig. 2a,b). As oxygen fugacity increases, iron shows a parabolic decrease from 3.35 wt. % at Co-CoO to 1.57 wt. % at HM (Fig. 2a). The opposite dependence is observed for V (Fig. 2b), with higher concentrations under more oxidised conditions ( $1443 \pm 61$  ppm at HM), compared to  $268 \pm 49$  ppm at Co-CoO. Over the same range in oxygen fugacity, magnetite compositions remain comparatively constant, with  $6.89 < \text{V}_2\text{O}_3$  (wt. %)  $< 8.39$  and  $84.40 < \text{FeO}^{(\text{T})}$  (wt. %)  $< 86.23$ , and, when re-calculated for 3 cations/4 oxygens, correspond to coulsonite components ( $X_{\text{coul}}$ ) of 0.11 to 0.13 (Table 4). In the 1 atm experiment at FMQ-1, V is incompatible in magnetite, with  $\text{V}_2\text{O}_3 = 0.33 \pm 0.10$  wt. % ( $X_{\text{coul}} = 0.005$ ), compared to  $2.67 \pm 0.03$  wt. % in the melt.

### **V isotopic Compositions of solution standards and USGS Reference Materials**

The first assessment of the long-term reproducibility of BDH is  $\delta^{51}\text{V}_{\text{AA}} = -1.19 \pm 0.08\text{‰}$  ( $n \approx 1000$ ; Nielsen et al., 2011). Later studies are in excellent agreement with this value (Wu et al., 2016:  $\delta^{51}\text{V}_{\text{AA}} = -1.23 \pm 0.04\text{‰}$  ( $n=197$ ), Schuth et al., 2017;  $\delta^{51}\text{V}_{\text{AA}} = -1.22 \pm 0.04\text{‰}$  ( $n=10$ ), and Sossi et al. (2017),  $-1.10 \pm 0.08\text{‰}$ , ( $n=5$ ). Continual measurement of BDH at RSES, ANU over the time period of unknown samples measured in this study yields  $-1.13 \pm 0.06\text{‰}$  ( $n = 28$ ). This consistency attests to the capability of measuring V isotopes in a pure V solution using the ANU analytical protocol. These values compares well with the column-processed  $\text{V}_2\text{O}_3$  starting material (also BDH) and BDH solution, which give  $-1.17 \pm 0.16\text{‰}$  and  $-1.22 \pm 0.12\text{‰}$ , respectively. In addition, USGS reference materials were analysed to test the reproducibility and accuracy of the wet chemistry (sample dissolution and ion exchange purification). Standard data for USGS reference materials is in agreement with literature data (Table 5). In fact, BIR-1 agrees well in all laboratories that measured this standard, even though different combinations of medium and low resolution, wet and dry plasma,  $10^9$ ,  $10^{10}$ ,  $10^{12}$  resistors and different instruments (the Neptune and the Nu) were employed (Table 5). The same is true of BCR-2, with the exception of the heavier value of  $-0.78 \pm 0.04\text{‰}$  reported by Wu et al. (2016). The stability of V isotope compositions processed using ion exchange chromatography across numerous labs employing diverse analytical protocols testifies to the robustness of the values reported herein.

### **V isotopic composition of magnetite and glass in experimental charges**

Vanadium isotope compositions of separated magnetite and glass are listed in Table 6. The V isotope composition of the starting material (BDH) is  $\delta^{51}\text{V}_{\text{AA}} = -1.19 \pm 0.08\text{‰}$  (Nielsen et al., 2011). In most cases, measured magnetite compositions are marginally heavier than this value, from  $-1.35 \pm 0.06\text{‰}$  to  $-1.48 \pm 0.07\text{‰}$ , while magnetite in the NNO experiment has  $-1.79 \pm 0.06\text{‰}$ . The glass phase is always systematically heavier than its coexisting magnetite, between  $-0.88 \pm 0.09\text{‰}$  to  $-1.16 \pm 0.09\text{‰}$ , again

close to the starting composition, but clearly resolved from magnetite. Measured isotope differences between magnetite and glass vary between  $-0.32 \pm 0.11\text{‰}$  and  $-0.70 \pm 0.08\text{‰}$ .

## Discussion

### Correcting for contamination and open-system behaviour of V in experiments

The time required to achieve isotopic equilibrium may be tested by performing a time-series, whereby all other variables are held constant aside from the run duration. Here, two experiments were run for three days (Co-CoO and HM), whereas the Re-ReO<sub>2</sub> and NNO experiments were run for 7 and 14 days, respectively. The coherence of all four experiments with one another in chemical and isotopic trends (Fig. 1a,b, Fig. 2) suggests attainment of isotopic equilibrium with run times longer than three days. Additionally, as magnetite was grown from oxide powders rather than equilibrated, grain growth should occur in equilibrium with the melt.

Diffusion rates for V<sup>4+</sup>, presumed to be the most abundant V species in the melt (*e.g.* Toplis and Corgne, 2002) are estimated with the empirical, viscosity-based model of Mungall (2002). At 1073K and 5 kb, and an average XH<sub>2</sub>O = 23.1 (mol. %) the calculated  $\log \eta = 3.7$  (Pa.s; Ardia et al., 2008), gives rise to V diffusivity of  $3.0 \times 10^{-10}$  cm<sup>2</sup>/s. For an inner capsule radius of 1.5 mm, equilibration times over the length scale of the capsule are 8.7 days (3 days gives equilibration length scales of 0.9 mm). These timescales are sufficient for equilibration over the length scale of melt-magnetite equilibrium, which occurs over 100-200  $\mu\text{m}$  (Fig. 1).

Despite evidence for equilibrium, open system behaviour, resulting from the loss of vanadium from either the melt or magnetite, must be evaluated. The most likely culprits are a) complexation of V by a fluid phase and b) alloying of V with the <sup>75</sup>Ag-<sup>25</sup>Pd capsule. The recovered charges are unvesiculated (Fig. 1) and have lower water contents than required for fluid saturation, obviating loss of V in a fluid phase. While V is immiscible in Ag (Smith, 1989), it readily forms alloys with Pd (Massalski, 1990). However, the low temperatures, high *f*O<sub>2</sub> and high Ag proportion in the Ag-Pd alloy minimise V loss to the inner capsule. The degree to which V loss affected each experiment may be quantified by mass balance. Re-constructed total V<sub>2</sub>O<sub>3</sub> contents, considering that 50% of the mix is comprised of magnetite (differential dissolution of magnetite into melt at different *f*O<sub>2</sub> has no effect on the calculated proportions), are given in Table 6. With the exception of the NNO run ( $3.41 \pm 0.16$  wt. %) all experiments are within uncertainty of the 4 wt. % in the starting mix. The 1 atm experiment yielded  $1.82 \pm 0.06$  wt. % V<sub>2</sub>O<sub>3</sub>, compared with the 2 wt. % in the starting mix, and it is noteworthy that the magnitude of the V isotope fractionation factor in this experiment is consistent with the high pressure experiments. Therefore, with the exception of the NNO run, which lost <15% V, the experiments acted as closed systems with respect to V.

To quantify the purity of the separated glass and magnetite fractions, V concentrations from a split of the solutions measured for their isotope composition are reported in Table 6. As the end-member phase compositions are known, mass balance constrains the fraction of magnetite contaminating the glass and is used to yield the isotope composition of the glass:

$$\delta^{51}V_{gl} = \frac{\delta^{51}V_{mix}(f_{mag}X_{mag}^V + (1-f_{mag})X_{gl}^V)}{f_{mag}\delta^{51}V_{mag}X_{mag}^V + (1-f_{mag})X_{gl}^V}. \quad (7)$$

Where  $X$  refers to the concentration of vanadium in magnetite and glass, and  $f$  their mass fraction. The mass fraction of magnetite is given by the two-phase mass balance:

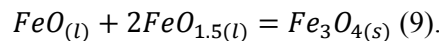
$$f_{mag} = \frac{(X_{mix}^V - f_{gl}X_{gl}^V)}{X_{mag}^V} \quad (8)$$

where  $X_{mix}^V$  is the concentration of V measured in solution. Values of  $X_{mix}^V$ , the total  $V_2O_3$  in the mixture and those calculated for  $f_{mag}$  are listed in Table 6, with  $f_{mag}$  ranging from 5.3% in the HM experiment, and 0.4% in the NNO run, where the long run time permitted growth of magnetite and facilitated separation from the glass. The corrected  $\delta^{51}V_{gl}$  values are in the range -1.02‰ (NNO) to -0.57‰ (HM) (Table 6). The true fractionation factor between magnetite and silicate glass ( $\Delta^{51}V_{mag-gl}$ ) can then be calculated (Table 6).

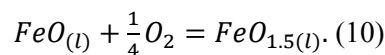
This quantity shows a negative dependence on the  $\log fO_2$  of the experiment at 800°C, where  $\Delta^{51}V_{mag-gl} = -0.92 \pm 0.11$ ‰ at  $\log fO_2 = -9.68$  (HM) and where  $\Delta^{51}V_{mag-gl} = -0.63 \pm 0.09$ ‰ at  $\log fO_2 = -15.74$  (FMQ-1), 1SD.

### Partitioning and redox-dependence of Fe and V

Quantification of the co-ordination and oxidation state of V, in both magnetite and melt, is essential to understanding the direction and magnitude of isotopic fractionation between two phases. At equilibrium, the reaction describing the formation of magnetite from iron oxides present in a silicate melt is:



This demonstrates that the stoichiometry of Fe in magnetite is fixed and does not therefore depend on  $fO_2$ . However, the relative proportions of the liquid components,  $FeO_{(l)}$  and  $FeO_{1.5(l)}$ , depend on  $fO_2$  according to the reaction:



Assuming ideal (two-site) mixing for  $Fe_3O_{4(s)}$ , as is the case at high temperatures where  $Fe^{2+}$  and  $Fe^{3+}$  are randomly distributed over the A and B sites of magnetite (Wu and Mason, 1981), then  $a(Fe_3O_4) = X(Fe_3O_4)^2$ . Therefore, at equilibrium, equation (9) is written:

$$0 = 2\log X(Fe_3O_4) - 2\log X(FeO_{1.5}) - \log X(FeO) - \log K_{(1)}^*, \quad (11)$$

and for equation (10)

$$0 = \log X(FeO_{1.5}) - 0.25\log f(O_2) - \log X(FeO) - \log K_{(2)}^* \quad (12)$$

where  $\log K^*$  denotes the deviation of the liquid components from ideality relative to the ideal case,  $\log K$ , in which  $a = X$ . Here, Henry's Law behaviour is assumed, such that  $\frac{\gamma_{FeO_{1.5}}}{\gamma_{FeO}}$  is constant over all  $fO_2$ , a condition shown to be valid for MORB (Berry et al., 2017).

With the constraint that  $X(FeO_{1.5}) + X(FeO) = \sum FeO_x$ , and given that  $\sum FeO_x$ ,  $X(Fe_3O_4)$  and  $fO_2$  are known from the experiments, a weighted non-linear least squares chi-squared minimisation is performed for the difference between the modelled and measured  $\sum FeO_x$  by changing  $\log K_{(9)}^*$  and  $\log K_{(10)}^*$  and hence  $X(FeO_{1.5})$  and  $X(FeO)$ :

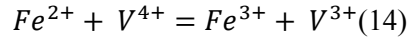
$$\chi^2 = \sum_i \left( \frac{\sum FeO_x^{calc} - \sum FeO_x^{obs}}{s(FeO_x)} \right)^2, \quad (13)$$

Where  $i$  denotes that the sum was performed globally for all four experiments simultaneously. The weighting of the uncertainty on the analyses,  $s(FeO_x)$  was set to 0.15 of the  $\sum FeO_x^{obs}$  value.

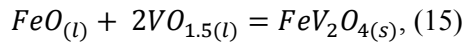
The calculated  $\log K_{(9)}^* = 6.34 \pm 0.30$  and  $\log K_{(10)}^* = 2.97 \pm 0.08$ . The high  $\log K_{(10)}^*$  relative to that determined for MORB at 1400°C and 1 bar (0.54; Berry et al., 2018), predominantly reflects the temperature-dependence of  $fO_2$ . Corrected to a mineral buffer (FMQ; Fig. 3a),  $Fe^{3+}/\sum Fe$  remains higher at a given  $fO_2$  in hydrous haplogranite relative to MORB. In fact, the high  $\log K_{(10)}^*$  is close to that found for the  $K_2Si_3O_7$  and  $Na_2Si_3O_7$  liquids studied at 1250°C and 1 bar by Knipping et al. (2015), suggesting that network-modifiers (Na, K) stabilise  $Fe^{3+}$  in silica-rich compositions (Thornber et al., 1980; Borisov et al., 2017).

Previous studies emphasise that trivalent V is significantly more compatible than  $V^{4+}$  or  $V^{5+}$  in silicate and oxide minerals (Canil, 1999; Nielsen et al., 1994; Richter et al., 2006b; Toplis and Corgne, 2002). This is due to the high octahedral site preference energy of  $V^{3+}$  ( $4/5\Delta_{oct}$ ) and the suitability of its ionic radius in VI-fold co-ordination (0.645 Å) for  $^{VI}Fe^{3+}$ -occupied sites (0.64 Å). Magnetite, which has an inverse-spinel cation distribution at room temperature,  $^{IV}Fe^{2+}^{VI}(Fe^{2+}, Fe^{3+})O_4$  (e.g., Bosi et al., 2009; Fleet, 1981), tends towards a random (normal) structure at high temperatures (Wu and Mason, 1981), and V is incorporated as the coulsonite end-member, which is a normal spinel;  $^{IV}Fe^{2+}^{VI}(V^{3+})_2O_4$

(Radtke, 1962). With both the ferric-ferrous and  $V^{3+/4+}$  redox pairs present, the following reaction occurs in magnetite:



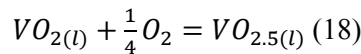
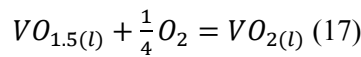
At high temperatures, the equilibrium constant tends to 1 (a statistically random arrangement) because having substantial fractions of each of the four species results in particularly high configurational entropy. As the free energy associated with electron exchange is small, this causes a large, negative deviation from ideality of mixing, meaning the substitution of  $V^{3+}$  in magnetite is energetically more favourable than either of the end-members ( $Fe_3O_4$  or  $FeV_2O_4$ ). As temperature decreases, the reactants become progressively favoured (Wakihara and Katsura, 1971; O'Neill and Navrotsky, 1984), and the substitution of V into magnetite can be written:



demonstrating that the incorporation of V is also independent of  $fO_2$ . At equilibrium, in the system Fe-V-O, eq. 15 becomes:

$$0 = 2\log(1 - XFe_3O_4) - 2\log X(VO_{1.5}) - \log X(FeO) - \log K_{(7)}^*. \quad (16)$$

The mole fraction of  $VO_{1.5}$  in the silicate melt, and resultant  $V^{3+}/V^{4+}$  ratio, is in turn dependent on the  $fO_2$  of the experiment:



and, at equilibrium:

$$0 = \log X(VO_2) - 0.25 \log f(O_2) - \log X(VO_{1.5}) - \log K_{(17)}^*. \quad (19)$$

$$0 = \log X(VO_{2.5}) - 0.25 \log f(O_2) - \log X(VO_2) - \log K_{(18)}^*. \quad (20)$$

As V is a trace element in the silicate melt, it is assumed to be in the Henry's Law region, where the activity coefficient for each valence is independent of  $fO_2$ . The constraint that  $X(VO_{1.5}) + X(VO_2) + X(VO_{2.5}) = \sum VO_x$  enables a global non-linear least-squares fit to be performed to the  $\sum VO_x$  measured in the silicate melt, analogous to that described for iron (eq. 13). Calculated equilibrium constants are  $\log K_{(15)}^* = 11.09 \pm 0.19$ ;  $\log K_{(17)}^* = 5.04 \pm 0.12$  and  $\log K_{(18)}^* = 2.65 \pm 0.10$ . The high equilibrium constant of eq. 15 reflects the stability of the  $FeV_2O_4$  component in magnetite. The  $\log K_{(17)}^* - \log K_{(18)}^* = 2.39$  shows that  $V^{4+}$  is the dominant oxidation state of V in silicate liquids (*e.g.* Giuli *et al.*, 2004; Sutton *et al.*, 2005), except under highly oxidising conditions ( $>FMQ+3$ ; Table 7, Fig. 3b).

Values of  $\log K^*$  in this work are generally lower (i.e., favouring the reduced species) than found in Toplis and Corgne (2002) for a ferrobasaltic composition at 1068°C and 1 bar, see Table 7. This behaviour is a reflection of the lower slope in a  $\log(D_V)$  vs.  $\Delta FMQ$  diagram (Fig. 4), where  $m$ , the slope, is dictated by the change of speciation of V in the liquid (a slope of -0.31 denotes  $\sum D_V = D_{V^{3+}}$ , with lower slopes reflecting increasing  $D_{V^{4+}}$ ). For the data of Toplis and Corgne (2002)  $m = -0.30$  compared with -0.16 herein. However, we note that the omission of their most oxidised experiment would decrease their slope to -0.18, in much closer agreement with our data. This reduction in slope equates to  $D_{V^{3+}} = 3070$  and  $D_{V^{4+}} = 64$ , hence  $D_{V^{4+}}/D_{V^{3+}} = 2.1\%$ , somewhat higher than the 0.2-0.5% (or 1% for a slope of -0.18) obtained by Toplis and Corgne (2002). By contrast, the slope of the data defined by the data of Sievwright *et al.*, (2017) for andesitic-dacitic melts at 1070°C, 1 bar and Arató and Audétat (2017) are steeper again, near -0.50; higher than the maximum of -0.30 allowed. Nevertheless, especially at high  $fO_2$ , our values of  $D_V$  compare well with Arató and Audétat (2017), whose experiments were run under essentially the same conditions (800°C, 5 kb) and compositions (haplogranite with ASI of  $\approx 1$ ). A slope of -0.50 implies that vanadium is exclusively  $V^{3+}$  in magnetite and  $V^{5+}$  in the melt. This differing behaviour may arise due to the high  $FeV_2O_4$  component in our experiments and those of Toplis and Corgne (2002), compared with the trace amount of V present in magnetite in Sievwright *et al.*, (2017) and Arató and Audétat (2017), where increasing  $V^{3+}$  pushes equilibrium (14) to the left, producing  $V^{4+}$ . In natural titanomagnetites crystallising from layered mafic intrusions (*e.g.*, Balan *et al.*, 2006)  $V^{3+}/\Sigma V$  ranges from 0.83 to 0.98, consistent with the preference of  $V^{3+}$  for magnetite. Together, these results confirm that  $D_{V^{3+}} \gg D_{V^{4+}}$  as expected thermodynamically.

### Controls on V isotope fractionation

Isotopic fractionation can be understood in the context of the bond valence model, which states that the sum of the bond valence ( $s = \text{charge/co-ordination}$ ) must equal the formal charge on the ion (Pauling, 1929). Its relation to the strength of the  $\langle V-O \rangle$  bonds (the parameter that controls isotope fractionation) is given by the force constant,  $K_f$ , which may be approximated by describing the bonding environment of V by electrostatic interactions, using the Born-Landé equation (see Young *et al.*, 2009; Sossi and O'Neill, 2017):

$$K_{f,V,O} = -\frac{\bar{s}_V \bar{s}_O q^2 (1 - n)}{4\pi \epsilon_0 r^3} \quad (21)$$

Here,  $\epsilon_0$  is the permittivity of free space,  $q$  the charge on an electron in coulombs,  $B$  the Born exponent (=12 in minerals, Young *et al.*, 2009) and  $r$  the radius in metres. The force constant therefore increases (which favours heavier isotopes) as charge increases or co-ordination decreases because both phenomena are associated with a shortening of the bond length.

Calculations performed herein are benchmarked against recent molecular dynamics simulations of hydrated V species of variable oxidation state (Wu et al., 2015) and compare favourably (see Appendix A for details). At high temperatures, the force constant can be related to the reduced partition function ratio, or  $\beta$  factor, by a constant term,  $f$  that describes the quantum component of the partition function ratio, and is dependent on the relative mass difference between the two isotopes (Bigeleisen and Mayer, 1947):

$$f = \frac{3N_A 10^3}{96\pi^2} \left( \frac{h}{k_B T} \right)^2 \left( \frac{1}{m_n} - \frac{1}{m_d} \right), \quad (22)$$

where  $N_A$  is Avogadro's number,  $h$  is Planck's constant,  $k_B$  Boltzmann's constant,  $m$  the molar mass, and for  $^{51}\text{V}/^{50}\text{V} = 1720$ ; and the temperature, in Kelvin, squared:

$$10^3 \ln \beta_V^{51/50} = \frac{1720(K_f)}{T^2}. \quad (23)$$

While the oxidation state of V in magnetite and co-existing melt can be estimated (see *Partitioning and redox-dependence of Fe and V*), information on co-ordination number and bond lengths is rare (Schindler et al., 2000). As in minerals,  $\text{V}^{3+}$  is octahedrally co-ordinated in basaltic glasses,  $\text{V}^{4+}$  has an average co-ordination of 5.33 (Sutton et al., 2005), whereas  $\text{V}^{5+}$ -O bond lengths are 1.82 Å (close to V-fold), decreasing to 1.7±0.02 Å (IV-fold) in alkali- and Ca-rich compositions (Giuli et al., 2004). This figure closely matches that obtained by adding the ionic radii of  $^{\text{IV}}\text{V}^{5+}$  (0.355 Å) and  $\text{O}^{2-}$  (1.38 Å), 1.74 Å. In the experimental glasses  $r$  is therefore estimated by linear interpolation between  $\langle \text{V-O} \rangle$  bond distances for  $\text{V}^{5+}$  ( $r = 1.74$  Å) and  $\text{V}^{4+}$  ( $r = 1.87$  Å) (Giuli et al., 2004; Sutton et al., 2005), with values shown in Table 8.

The constancy of V oxidation state, and hence calculated  $\langle \text{V-O} \rangle$  bond lengths in magnetite over the range of  $f\text{O}_2$  investigated means that changes in V speciation in the melt control the degree of isotopic fractionation. Results of these calculations (Fig. 5) show that an average oxygen co-ordination of 2.5 best fits the melt experimental data, implying a network-forming role for both  $\text{V}^{4+}$  and  $\text{V}^{5+}$ , which is unsurprising given their similar charge and co-ordination to  $\text{Si}^{4+}$ . Importantly, the model also predicts that magnetite, where V exists in a lower average valence (3+) and higher co-ordination (VI-fold), should always be isotopically *lighter* than co-existing melt. The model reproduces the larger isotopic fractionation observed in the more oxidised experiments, where the difference in charge, co-ordination and  $\langle \text{V-O} \rangle$  bond length is greater between the two phases at higher  $f\text{O}_2$ .

Figure 5 illustrates the dependence of the fractionation factor between magnetite and melt as a function of  $f\text{O}_2$  at 800°C, which has the form:

$$\Delta^{51}\text{V}_{\text{Mag-Melt}} (\text{‰}) = -0.045 \pm 0.021(\Delta FMQ) - 0.70 \pm 0.05 \quad (24)$$

Uncertainties take into account the errors on the analyses themselves as well as the goodness of fit of the regression, and should be noted that they are compensatory (a positive uncertainty in the slope is compensated for by a negative uncertainty in the intercept, and vice-versa). The slope illustrates that the dependence on  $fO_2$  is small over the range of igneous rocks as V remains  $V^{3+}$  in magnetite but increases in valence in the melt. Fractionation is largely driven by i) the difference in redox state of trivalent V in magnetite and  $V^{4+}/V^{5+}$  in the melt over a range of  $fO_2$ , and ii) the difference in co-ordination between octahedral  $V^{3+}$  in magnetite and IV- to V-fold co-ordinated V in the liquid.

## Implications

### Comparison with natural data

Minerals in the titanomagnetite solid solution are common accessory phases in igneous systems on Earth. Despite their minor abundance, the timing of their appearance on the liquid line of descent gives rise to the distinct chemical evolution of the tholeiitic (late saturation, iron-enrichment) and calc-alkaline (early saturation, iron depletion) magmatic trends (Sisson and Grove, 1993). As the timing of this saturation is dependent on the  $fO_2$  of the crystallising magma (e.g., Toplis and Carroll, 1995; Feig et al., 2010), magnetite may provide an important record of the prevailing oxygen fugacity via its vanadium isotope composition. Furthermore, magnetite crystallisation reduces the melt by preferentially sequestering  $Fe^{3+}$  and can trigger sulphide saturation with important implications for the formation of economically viable mineral deposits (e.g., Jenner et al., 2010).

Prytulak et al. (2017) measured the whole rock V isotope composition of two differentiating magmatic suites from Hekla, Iceland and Anatahan volcano, from the Marianas island arc. The former records  $fO_2 \approx FMQ$  (Baldrige, 1974) whereas magmas from the Marianas crystallise under a more oxidised regime, near FMQ+2 (Brounce et al., 2014). Despite these differing oxygen fugacities, the V isotope evolution in both systems shows a similar trajectory, in which the most differentiated magmas reach  $\delta^{51}V_{AA} \sim +1\text{‰}$  from an initial, parent magma composition of near  $-0.7\text{‰}$ . In detail, the calculated magnetite-melt fractionation factors differ slightly;  $-0.5\text{‰}$  for Anatahan, and  $-0.45\text{‰}$  for Hekla (Prytulak et al., 2017) at  $\approx 1000^\circ\text{C}$ .

Strikingly, however, both of these fractionation factors derived from bulk lavas fall in the range determined experimentally herein. Using the correlation of the experimental fractionation factor with  $fO_2$  (eq. 24), corrected from  $800^\circ\text{C}$  to  $1000^\circ\text{C}$  assuming a  $1/T^2$  dependence (eq. 23), gives relative  $fO_2$  of FMQ-1.5 for Hekla and FMQ+0.7 for Anatahan, in excellent agreement with the 2 log unit difference recorded by oxygen barometry (see Prytulak et al., 2017, and references therein), although they are displaced to lower values (FMQ and FMQ+2, respectively). It remains to be explored as to whether changes in composition in the melt phase affect V redox and co-ordination, and hence the isotopic fractionation factor. That melt composition can alter co-ordination number was shown for Fe,



where IV-fold co-ordinated iron is preferred relative to VI-fold in more polymerised, alkali-rich rhyolitic compositions with respect to more mafic compositions (Dauphas et al. 2014). A similar effect may be expected for V, because the low bond valence alkalis stabilise lower V co-ordination numbers (see Jackson et al., 2005). Indeed, Giuli et al. (2004) observed that in Fe-bearing compositions,  $V^{5+}$  was in higher co-ordination than in Fe-free and sodium-silicate compositions. The stronger <V-O> bonds found in lower co-ordination environments would therefore produce greater  $\Delta^{51}V_{\text{mag-melt}}$  fractionation in granitic melts compared with basaltic liquids. Empirically, given the displacement in calculated  $fO_2$  with respect to measured values in Hekla and Anatahan suggests that the fractionation factor may indeed be sensitive to composition. If so, then the experimental calibration for haplogranitic compositions is not directly applicable to the andesitic-dacitic liquids crystallising at Hekla and Anatahan. Nevertheless, the  $fO_2$  dependence (the slope in eq. 24) will be less sensitive to composition because different melt components will affect the  $\log K^*$  of eqs. 15, 17 and 18 by altering the vanadium oxide activity coefficients in the melt ( $\gamma VO_{1.5}$ ,  $\gamma VO_2$  and  $\gamma VO_{2.5}$ ) but not the stoichiometries of the reactions.

The relative insensitivity of the V isotope composition in whole rock lavas to their different redox states shows that V isotopes are not straightforward indicators of  $fO_2$  variations in igneous systems. However, the systematic increase in fractionation factor with  $fO_2$  (Fig. 2), is potentially resolvable if magnetite-melt pairs are determined. In the absence of the melt phase, because magnetite commonly hosts the majority of the vanadium in crystallising magmas, it may act as a single mineral indicator of  $fO_2$ .

### **Magnetite as an indicator of $fO_2$**

Given the diverse ways in which magnetite may form on the Earth, the chemistry of this mineral likely holds clues to its provenance and conditions of formation. However, discrimination of magnetite provenance based trace elements alone can be troublesome given that igneous magnetite may span a wide range of composition dependent on its petrogenetic history, resulting in the overlap of many trace element fingerprints in different formation environments (e.g., Dare et al., 2012).

Magnetite from igneous rocks are amongst the most V-rich on Earth, often containing > 0.15 wt. %  $V_2O_3$ , and reaching levels of several weight percent in some settings such as layered mafic intrusions (e.g. Grigsby, 1990; Dare et al., 2014; Toplis and Corgne, 2002; Balan et al., 2006). Figure 6 depicts results of a fractional crystallisation model similar to Prytulak et al. (2017) to predict the V isotope composition of magnetite at different  $fO_2$  conditions. The  $fO_2$  of an initial ferrobaltic magma with 6.5 wt. % MgO, 12 wt. % FeO and 300 ppm V (Toplis and Corgne, 2002), is varied from FMQ-1, FMQ+1 to FMQ+3 (Fig. 6). Temperature is related to the fraction of melt,  $F$ , by the expression  $T^\circ C = 1022 + 266(F) - 290F^2 + 175F^3$  (Toplis and Corgne, 2002). Magnetite saturation (at  $T^\circ C <$

27.2 $\times$  $\Delta$ NNO+1125) and modal abundance (ol+plag):cpx:mag =42:40:18, as a function of  $fO_2$  and temperature, is parameterised after Toplis and Corgne (2002), while olivine and augite Mg#s are given by  $K_D^{Fe-Mg} = 0.3$  (Toplis, 2005; Bédard, 2010). Plagioclase is the only other mineral to crystallise, with phase proportions set to ol:plag = 0.27 and ol:(cpx+plag) = 0.27 (Toplis and Carroll, 1995). Partition coefficients as a function of  $fO_2$  for V in magnetite are taken from this work and those for clinopyroxene from Mallmann and O'Neill (2009). The vanadium isotope fractionation factor between magnetite and melt is taken from equation (24), and is assumed to apply to clinopyroxene-melt due to its preference for trivalent V in octahedral co-ordination (Karner et al., 2005; Mallmann and O'Neill, 2009). At FMQ-1, clinopyroxene crystallises first, depriving the melt of half its V budget before magnetite crystallises ( $D_V = 63.1$ ) with a maximum of 1.4 wt. %  $V_2O_3$ . Intermediate  $fO_2$  produces the greatest enrichment of V in magnetite (1.51 wt. %) despite lower  $D_V$ , of 26.9, as it co-crystallises with augite. At FMQ+3, magnetite is initially poor in  $V_2O_3$  (0.57 wt. %) owing to its lower  $D_V$  of 12.6, but the melt is depleted more slowly, such that magnetite crystallising at the end of differentiation is still V-rich (>100 ppm). Magnetite from the reduced series has the heaviest  $\delta^{51}V$ , owing to a) extraction of light V into clinopyroxene and b) rapid depletion of V from the melt (Fig. 6). In general, magmatic magnetite will be initially light and V-rich, before evolving to heavy, V-poor compositions due to progressive extraction of V by magnetite ( $\pm$ clinopyroxene).

Granitic rocks, whose compositions range from reduced, A-type granites (Turner et al., 1992; Frost and Frost, 2010) to oxidised, magnetite-bearing I-type granite (Chappell and White, 1977) may evolve distinct V isotope signatures in magnetite. Qualitatively, the protracted fractionation crystallisation that produces A-types (*e.g.*, Turner et al., 1992; Shellnutt et al., 2009) depletes the remaining melt in V and light V isotopes, such that any magnetite to crystallise from these evolved magmas is V-poor (<100 ppm) and inherits a heavy isotope composition, >1.5‰ (Fig. 6). By contrast, magnetite in I-type granites, owing to their more oxidising environment, crystallises earlier in its magmatic evolution while ample V remains in the melt. This melt is still isotopically light, akin to basaltic liquids (Prytulak et al., 2013; Fig. 6), and the  $\Delta^{51}V_{mag-melt}$  fractionation factor upon magnetite precipitation is enhanced due to the oxidising conditions, resulting in isotopically light magnetite,  $\leq 1\%$  (Fig. 6) that is relatively rich in V (>100 ppm). This behaviour mirrors that observed for iron isotopes in granitic rocks (Foden et al., 2015). The isotopic composition of V in detrital, igneous magnetite may therefore prove diagnostic in identifying the conditions under which it crystallised from its parent magma, which may be especially useful in older Archean rocks in which magnetite is often detrital.

Magnetite precipitated from high temperature (500 – 800 °C) porphyry fluids may reach similar  $V_2O_3$  contents ( $\approx 0.5$  wt. %; *e.g.* Nadoll et al., 2014) to those found in mafic igneous rocks. Vanadium contents decrease to  $\approx 0.1$  wt. % (Canil et al., 2016) in magnetite associated with skarn-type mineralisation (300 – 500°C). The lowest V contents (and trace elements in general) occur in

magnetite precipitated from seawater to comprise BIFs (Dare et al., 2014; Nadoll et al., 2014), with a median of 4.8 ppm ( $-4.5/+36$ ,  $n = 135$ ). The diversity of magnetite V concentrations forming in distinct environments at different temperatures offers ample scope for stable isotopic fractionation. Therefore, characterisation of the V isotope composition of magnetite formed in different settings may in the future, together with V concentrations, act as a powerful provenance tracer.

## Conclusion

The first V isotope fractionation factors between experimentally-grown magnetite and hydrous, haplogranitic melts at 800°C, 0.5 GPa were determined. Oxygen fugacity in the experiments was varied by fixing  $fH_2$  according to different mineral buffers, varying from FMQ-1 to FMQ+5, supplemented by a 1 atm run with an alkali-silica melt at FMQ-1. Vanadium becomes more compatible in magnetite at progressively more reducing conditions in response to a higher abundance of  $V^{3+}$  in the granitic melt. This behaviour is reflected in increasingly isotopically heavy melt relative to magnetite at higher  $fO_2$ , ranging from  $\Delta^{51}V_{mag-gl} = -0.63 \pm 0.09\text{‰}$  at FMQ-1 to  $-0.92 \pm 0.11\text{‰}$  at  $\approx$ FMQ+5, and can be fit by  $\Delta^{51}V (\text{‰}) = -0.045 \pm 0.021 \times \Delta FMQ - 0.70 \pm 0.05$ . Such a trend can be reproduced by modelling the fractionation factor according to the bond valence model, where V is  $VI V^{3+}$  in magnetite, and a mixture of IV- and VI-fold  $V^{5+}$  and  $V^{4+}$  in the melt. Experimentally-derived fractionation factors are in accord with those inferred from natural systems, highlighting the role of magnetite in controlling the V isotope composition of evolving magmatic systems. The ubiquity of magnetite on the Earth's surface and its formation in igneous, metamorphic, hydrothermal, and aqueous environments likely engenders significant isotopic fractionation.

## Acknowledgements

PAS was funded by an Australian Postgraduate Award and an ANU Vice-Chancellor's Scholarship. Analytical costs and JPs visit to ANU were funded by Australian Research Council Discovery Grant DP130101355 to H. St.C. O'Neill and J. Prytulak. Many thanks to Jeremy Wykes, Dave Clark and Dean Scott for discussions regarding the piston cylinder experiments, Graham Mortimer for facilitating the set-up of V isotopes at the RSES clean lab, and Les Kinsley for assistance and feedback on running V isotopes on the Neptune Plus. We greatly appreciate two thoughtful and comprehensive reviews by Alan Woodland and Dante Canil that helped improve many aspects of this study, and acknowledge perceptive comments from Adrian Fiege on an earlier version of this work. We are grateful to Othmar Müntener for his exemplary editorial handling.

## References

Anbar AD, Roe JE, Barling J, Nealson KH (2000) Nonbiological Fractionation of Iron Isotopes. *Science*, 288:126–128.

- Arató R, Audétat A (2017) Experimental calibration of a new oxybarometer for silicic magmas based on vanadium partitioning between magnetite and silicate melt. *Geochim Cosmochim Acta*, 209:284-295.
- Ardia P, Giordano D, Schmidt MW (2008) A model for the viscosity of rhyolite as a function of H<sub>2</sub>O-content and pressure: A calibration based on centrifuge piston cylinder experiments. *Geochim Cosmochim Acta*, 72:6103-6123.
- Balan E, De Villiers JPR, Eeckhout SG, Glatzel P, Toplis MJ, Fritsch E, Allard T, Galois L, Calas G (2006) The oxidation state of vanadium in titanomagnetite from layered basic intrusions. *Am Mineral* 91:953–956.
- Baldrige WS, McGetchin TR, Frey FA, Jarosewich E (1973) Magmatic evolution of Hekla, Iceland. *Contrib Mineral Petrol*, 42(3):245-258.
- Bédard JH (2010) Parameterization of the Fe-Mg exchange coefficient ( $K_D$ ) between clinopyroxene and silicate melts. *Chem Geol*, 274(3–4):169–176.
- Behrens H, Jantos N (2001) The effect of anhydrous composition on water solubility in granitic melts. *Am Mineral* 86(1–2):14–20.
- Berry AJ, Stewart GA, O'Neill HSC, Mallmann G, Mosselmans JFW (2018) A re-assessment of the oxidation state of iron in MORB glasses. *Earth Planet Sci Lett* 483:114–123.
- Bigeleisen J, Mayer MG (1947) Calculation of equilibrium constants for isotopic exchange reactions. *J Chem Phys*, 15(5):261-267.
- Boettcher AL, Mysen BO, Allen JC (1973) Techniques for the control of water fugacity and oxygen fugacity for experimentation in solid-media high-pressure apparatus. *J Geophys Res* 78:5898–5901.
- Borisov A, Behrens H, Holtz F (2017) Effects of strong network modifiers on Fe<sup>3+</sup>/Fe<sup>2+</sup> in silicate melts: an experimental study. *Contrib Mineral Petrol* 172(5):34.
- Bosi F, Halenius U, Skogby H (2009) Crystal chemistry of the magnetite-ulvöspinel series. *Am. Mineral.* 94:181–189.
- Boutroy E, Dare SAS, Beaudoin G, Barnes S-J, Lightfoot PC (2014) Magnetite composition in Ni-Cu-PGE deposits worldwide: application to mineral exploration. *J Geochem Exp* 145:64-81.
- Bowen NL, Schairer JF, Willems HVM (1930) The Ternary System Na<sub>2</sub>SiO<sub>3</sub>-Fe<sub>2</sub>O<sub>3</sub>-SiO<sub>2</sub>. *Am J Sci* 20:405–455.
- Brounce MN, Kelley KA, Cottrell E (2014) Variations in Fe<sup>3+</sup>/ΣFe of Mariana Arc Basalts and Mantle Wedge fO<sub>2</sub>. *J Petrol*, 55(12):2513-2536.
- Canil D (1997) Vanadium partitioning and the oxidation state of Archean komatiite magmas. *Nature*, 389:842-845.
- Canil D (1999) Vanadium partitioning between orthopyroxene, spinel and silicate melt and the redox states of mantle source regions for primary magmas. *Geochim Cosmochim Acta* 63:557–572.
- Canil D (2004) Mildly incompatible elements in peridotites and the origins of mantle lithosphere. *Lithos* 77:375–393.
- Canil D, Grondahl C, Lacourse T, Pisiak LK (2016) Trace elements in magnetite from porphyry Cu-Mo-Au deposits in British Columbia, Canada. *Ore Geol Rev* 72:1116-1128.
- Carmichael ISE (1991) The redox states of basic and silicic magmas: a reflection of their source regions? *Contrib to Mineral Petrol* 106:129–141.
- Chappell BW, White AJR (1974) Two contrasting granite types. *Pacific Geology* 8:173–174
- Chou I-M (1986) Permeability of precious metals to hydrogen at 2 kb total pressure and elevated temperatures. *Am J Sci* 286:638–658.
- Dare SAS, Barnes S-J, Beaudoin G (2012) Variation in trace element content of magnetite crystallized from a fractionating sulfide liquid, Sudbury, Canada: Implications for provenance discrimination. *Geochim Cosmochim Acta*, 88:27-50.

- Dare SAS, Barnes S-J, Beaudoin G, Meric J, Boutroy E, Potvin-Doucet C (2014) Trace elements in magnetite as petrogenetic indicators. *Miner Deposita*, 49:785-796.
- Dauphas N, Roskosz M, Alp EE, Neuville DR, Hu MY, Sio CK, Zhao J, Tissandier L, Médard E, Cordier C (2014). Magma redox and structural controls on iron isotope variations in Earth's mantle and crust. *Earth Planet Sci Lett*, 398:127-140.
- Eugster HP (1957) Heterogeneous Reactions Involving Oxidation and Reduction at High Pressures and Temperatures. *J Chem Phys* 26:1760–1761.
- Feig ST, Koepke J, Snow JE (2010) Effect of oxygen fugacity and water on phase equilibria of a hydrous tholeiitic basalt. *Contrib Mineral Petrol* 160(4):551-568.
- Fleet ME (1981) The Structure of Magnetite. *Acta Crystallogr B* 37:917–920.
- Frost CD, Frost BR (2010) On ferroan (A-type) granitoids: their compositional variability and modes of origin. *J Petrol*, 52(1):39-53.
- Fuchs JN (1825) Ueber ein neues Product aus Kieselerde und Kali. *Arch Für die gesammte Naturlehre* 5:385–412.
- Giuli G, Paris E, Mungall JE, Romano C, Dingwell DB (2004) V oxidation state and coordination number in silicate glasses by XAS. *Am Mineral* 89:1640–1646.
- Grigsby JD (1990) Detrital magnetite as a provenance indicator. *J Sediment Res* 60:940-951
- Holtz F, Johannes W, Tamic N, Behrens H (2001) Maximum and minimum water contents of granitic melts generated in the crust: a reevaluation and implications. *Lithos* 56:1–14.
- Jackson WE, Farges F, Yeager M, Mabrouk PA, Rossano S, Waychunas GA, Solomon EI, Brown Jr GE (2005) Multi-spectroscopic study of Fe (II) in silicate glasses: Implications for the coordination environment of Fe (II) in silicate melts. *Geochim Cosmochim Acta*, 69(17):4315-4332.
- Jarosewich E, Nelen JA, Norberg JA (1980). Reference Samples for Electron Microprobe Analysis. *Geostand Geoanalytical Res* 4:43–47.
- Jenner FE, O'Neill HSC, Arculus RJ, Mavrogenes JA (2010) The magnetite crisis in the evolution of arc-related magmas and the initial concentration of Au, Ag and Cu. *J Petrol*, 51(12):2445-2464.
- Karner J, Papike JJ, Shearer CK (2006) Comparative planetary mineralogy: Pyroxene major-and minor-element chemistry and partitioning of vanadium between pyroxene and melt in planetary basalts. *Am Mineral*, 91(10):1574-1582.
- Knipping JL, Behrens H, Wilke M, Goettlicher J, Stabile P (2015) Effect of oxygen fugacity on the coordination and oxidation state of iron in alkali bearing silicate melts. *Chem Geol* 411:143-154.
- Lee C-TA, Leeman WP, Canil D, Li ZXA (2005) Similar V/Sc Systematics in MORB and Arc Basalts: Implications for the Oxygen Fugacities of their Mantle Source Regions. *J Petrol* 46:2313–2336.
- Mallmann G, O'Neill HSC (2009) The Crystal/Melt Partitioning of V during Mantle Melting as a Function of Oxygen Fugacity Compared with some other Elements (Al, P, Ca, Sc, Ti, Cr, Fe, Ga, Y, Zr and Nb). *J Petrol* 50:1765–1794.
- Mallmann G, O'Neill HSC (2013) Calibration of an Empirical Thermometer and Oxybarometer based on the Partitioning of Sc, Y and V between Olivine and Silicate Melt. *J Petrol*, 54(5):933-949.
- Massalski TB (1990) Binary Alloy Phase Diagrams, 2<sup>nd</sup> ed. ASM International, Materials Park, Ohio.
- Matjuschkin V, Brooker RA, Tattitch B, Blundy JD, Stamper CC (2015) Control and monitoring of oxygen fugacity in piston cylinder experiments. *Contrib to Mineral Petrol*, 169:1-16.
- Medard E, McCammon CA, Barr JA, Grove TL (2008) Oxygen fugacity, temperature reproducibility, and H<sub>2</sub>O contents of nominally anhydrous piston-cylinder experiments using graphite capsules. *Am Mineral* 93:1838–1844.

- Muan A (1963) Silver-Palladium Alloys As Crucible Material in Studies of Low-Melting Iron Silicates. *Ceram Bull* 42:344–347.
- Mungall JE (2002) Empirical models relating viscosity and tracer diffusion in magmatic silicate melts. *Geochim Cosmochim Acta*, 66(1):125-143.
- Nadoll P, Angerer T, Mauk JL, French D, Walshe J (2014) The chemistry of hydrothermal magnetite: a review. *Ore Geol Rev* 16:1-32.
- Nielsen RL, Forsythe LM, Gallahan WE, Fisk MR (1994) Major- and trace-element magnetite-melt equilibria. *Chem Geol* 117:167–191.
- Nielsen SG, Prytulak J, Halliday AN (2011) Determination of Precise and Accurate  $^{51}\text{V}/^{50}\text{V}$  Isotope Ratios by MC-ICP-MS, Part 1: Chemical Separation of Vanadium and Mass Spectrometric Protocols. *Geostand Geoanalytical Res* 35:293–306.
- Nielsen SG, Prytulak J, Wood BJ, Halliday AN (2014) Vanadium isotopic difference between the silicate Earth and meteorites. *Earth Planet Sci Lett* 389:167-175.
- Nielsen SG, Owens JD, Horner TJ (2016) Analysis of high-precision vanadium isotope ratios by medium resolution MC-ICP-MS. *J Anal At Spectrom*, 31:531-536
- O'Neill HSC, Navrotsky A (1984) Cation distributions and thermodynamic properties of binary spinel solid solutions. *Am Mineral* 69:733–753.
- O'Neill HSC (1987) Quartz-fayalite-iron and quartz-fayalite-magnetite equilibria and the free energy of formation of fayalite ( $\text{Fe}_2\text{SiO}_4$ ) and magnetite ( $\text{Fe}_3\text{O}_4$ ). *Am Mineral* 72(1-2):67-75.
- Parkinson IJ, Arculus RJ (1999) The redox state of subduction zones: insights from arc-peridotites. *Chem Geol* 160:409–423.
- Pauling L, (1929) The Principles Determining the Structure of Complex Ionic Crystals. *J Am Chem Soc* 51:1010–1026.
- Petric A, Jacob KT (1982). Thermodynamic Properties of  $\text{Fe}_3\text{O}_4$ -  $\text{FeV}_2\text{O}_4$  and  $\text{Fe}_3\text{O}_4$ -  $\text{FeCr}_2\text{O}_4$  Spinel Solid Solutions. *J Am Ceram Soc* 65(2):117-123.
- Prytulak J, Nielsen SG, Halliday AN (2011) Determination of Precise and Accurate  $^{51}\text{V}/^{50}\text{V}$  Isotope Ratios by Multi-Collector ICP-MS, Part 2: Isotopic Composition of Six Reference Materials plus the Allende Chondrite and Verification Tests. *Geostand Geoanalytical Res* 35:307–318.
- Prytulak J, Nielsen SG, Ionov DA, Halliday AN, Harvey J, Kelley KA, Niu Y, Peate DW, Shimizu K, Sims KWW (2013) The stable vanadium isotope composition of the mantle and mafic lavas. *Earth Planet Sci Lett* 365:177–189.
- Prytulak J, Sossi PA, Halliday AN, Plank T, Savage PS, Woodhead JD (2017) Stable vanadium isotopes as a redox proxy in magmatic systems? *Geochem Persp Lett*, 3(1):75-84.
- Radtke AS (1962) Coulsonite,  $\text{FeV}_2\text{O}_4$ , A Spinel-Type Mineral from Lovelock, Nevada. *Am Mineral* 47:1284–1291.
- Righter K, Sutton SR, Newville M, Le L, Schwandt C, Uchida H, Lavina B, Downs RT (2006a) An experimental study of the oxidation state of vanadium in spinel and basaltic melt with implications for the origin of planetary basalt. *Am Mineral* 91, 1643–1656.
- Righter K, Leeman W, Hervig R (2006b) Partitioning of Ni, Co and V between spinel-structured oxides and silicate melts: Importance of spinel composition. *Chem Geol* 227:1–25.
- Schauble E (2004) Applying stable isotope fractionation theory to new systems. *Rev Mineral Geochem* 55:65-111.
- Schindler M, Hawthorne FC, Baur WH (2000) Crystal Chemical Aspects of Vanadium: Polyhedral Geometries, Characteristic Bond Valences, and Polymerization of (Von) Polyhedra. *Chem Mater* 12:1248–1259.

- Schuth S, Horn I, Brüske A, Wolff PE, Weyer S (2017) First vanadium isotope analyses of V-rich minerals by femtosecond laser ablation and solution-nebulization MC-ICP-MS. *Ore Geo Rev*, 81:1271-1286.
- Shannon RT (1976) Revised effective ionic radii and systematic studies of interatomic distances in halides and chalcogenides. *Acta Crystall A*, 32(5):751-767.
- Shellnutt JG, Zhou MF, Zellmer GF (2009) The role of Fe–Ti oxide crystallization in the formation of A-type granitoids with implications for the Daly gap: an example from the Permian Baima igneous complex, SW China. *Chem Geol*, 259(3-4):204-217.
- Sievwright RH, Wilkinson JJ, O'Neill, HSC, Berry AJ (2017) Thermodynamic controls on element partitioning between titanomagnetite and andesitic–dacitic silicate melts. *Contrib Mineral Petrol* 172(8):62.
- Sisson TW, Grove TL (1993) Experimental investigations of the role of H<sub>2</sub>O in calc-alkaline differentiation and subduction zone magmatism. *Contrib Mineral Petrol*, 113(2):143-166.
- Smith JF (1989) Phase Diagrams of Binary Vanadium Alloys, in: Monograph Series on Alloy Phase Diagrams. ASM International, Materials Park, Ohio, p. 251.
- Sossi PA, Halverson GP, Nebel O, Eggins SM (2015) Combined Separation of Cu, Fe and Zn from Rock Matrices and Improved Analytical Protocols for Stable Isotope Determination. *Geostand Geoanalytical Res* 39(2):129-149
- Sossi PA, O'Neill HSC (2017) The effect of bonding environment on iron isotope fractionation between minerals at high temperature. *Geochim Cosmochim Acta*, 196:121-143
- Sossi PA, Moynier F, Chaussidon M, Villeneuve J, Kato C, Gounelle M (2017) Early Solar System irradiation quantified by linked vanadium and beryllium isotope variations in meteorites. *Nature Astronomy*, 1:0055.
- Sutton SR, Karner J, Papike J, Delaney JS, Shearer C, Newville M, Eng P, Rivers M, Dyar MD (2005) Vanadium K edge XANES of synthetic and natural basaltic glasses and application to microscale oxygen barometry. *Geochim Cosmochim Acta* 69:2333–2348.
- Thornber CR, Roeder PL, Foster JR (1980) The effect of composition on the ferric-ferrous ratio in basaltic liquids at atmospheric pressure. *Geochim Cosmochim Acta*, 44(3):525-532.
- Toplis MJ, Carroll MR (1995) An experimental study of the influence of oxygen fugacity on Fe-Ti oxide stability, phase relations, and mineral—melt equilibria in ferro-basaltic systems. *J Petrol*, 36(5):1137-1170.
- Turner SP, Foden JD, Morrison RS (1992) Derivation of some A-type magmas by fractionation of basaltic magma: an example from the Padthaway Ridge, South Australia. *Lithos*, 28(2):151-179.
- Toplis MJ, Corgne A (2002) An experimental study of element partitioning between magnetite, clinopyroxene and iron-bearing silicate liquids with particular emphasis on vanadium. *Contrib to Mineral Petrol* 144:22–37.
- Urey HC (1947) The thermodynamic properties of isotopic substances. *J Chem Soc*, 562-581.
- Woodland AB, O'Neill HSC (1997) Thermodynamic data for Fe-bearing phases obtained using noble metal alloys as redox sensors. *Geochim Cosmochim Acta* 61:4359–4366.
- Wu C, Mason T O (1981) Thermopower measurement of cation distributio in magnetite. *J Am Ceram Soc* 64(9):520-522
- Wu F, Qin T, Li X, Liu Y, Huang JH, Wu Z, Huang F (2015) First-principles investigation of vanadium isotope fractionation in solution and during adsorption. *Earth Planet Sci Lett*, 426:216-224.
- Wu F, Qi Y, Yu H, Tain S, Hou Z, Huang F (2016) Vanadium isotope measurement by MC-ICP-MS. *Chem Geol*, 421:17-25.
- Young ED, Tonui E, Manning CE, Schauble EA, Macris CA (2009) Spinel–olivine magnesium isotope thermometry in the mantle and implications for the Mg isotopic composition of Earth. *Earth Planet Sci Lett* 288:524–533

## Figure Captions

**Fig. 1** Back-scattered electron image of experimental run D1555 (Re-ReO<sub>2</sub>). Bright crystals are magnetite, while the darker regions are glass.

**Fig. 2** The concentration of **a)** FeO (wt. %) and **b)** V (ppm) measured in the glass by EPMA as a function of  $f\text{O}_2$ . Error bars on symbols are 1SD

**Fig. 3** The control of  $\log f\text{O}_2$  (expressed relative to the FMQ buffer,  $\Delta\text{FMQ}$ ; O'Neill, 1987) on the relative proportions of redox-sensitive species for **a)**  $\text{Fe}^{2+}/\text{Fe}^{3+}$ . Compositions are hydrous haplogranite (orange curve, this work),  $(\text{Na,K})_2\text{Si}_3\text{O}_7$  liquids (Knipping et al., 2015) and Mid-Ocean Ridge Basalt, MORB (Berry et al., 2018). Numbers refer to the  $\log K^*$  value of reaction 10. **b)**  $\text{V}^{3+}/\text{V}^{4+}/\text{V}^{5+}$ . The relative abundance of vanadium species is shown by the red line ( $\text{V}^{3+}$ ), green line ( $\text{V}^{4+}$ ) and blue line ( $\text{V}^{5+}$ ) for the hydrous haplogranite composition (this work), calculated from values of the equilibrium constants for reactions 15, 17 and 18. See *Partitioning and redox-dependence of Fe and V*.

**Fig. 4** The change in the logarithm of the bulk partition coefficient of vanadium between magnetite and melt ( $\log D_V$ ) as a function of  $\log f\text{O}_2$ , relative to the FMQ buffer ( $\Delta\text{FMQ}$ ; O'Neill, 1987). Plotted are datasets for different melt compositions; ferrobasalt at 1068°C, 1 bar (green, Toplis and Corgne, 2002); andesite-dacite at 1070-1120°C, 1 bar (Sievwright et al., 2017), and hydrous haplogranite at 800°C, 5 kb (blue, Arató and Audétat, and red, this work). The slope of the curve is proportional to the relative compatibility of  $\text{V}^{3+}$  over  $\text{V}^{4+}$ , see *Partitioning and redox-dependence of Fe and V*.

**Fig. 5** Measured vanadium isotope fractionation factor between magnetite and melt and its evolution with  $f\text{O}_2$  at 800°C. Fits to the data are *i)* a linear regression (dashed line) and associated 1SD confidence envelope (grey field), which corresponds to eq. 24, and *ii)* calculations based on the bond valence model (solid line). See *Controls on V isotope fractionation*.

**Fig. 6** The variation of  $\delta^{51}\text{V}_{\text{AA}}$  with V content (expressed as  $\text{V}_2\text{O}_3$  wt. % on a logarithmic scale) in magnetite and melt. Three models of an evolving ferrobasaltic magma are presented at FMQ-1 (red), FMQ+1 (green) and FMQ+3 (blue). The solid lines denote the composition of the magnetite and the associated magmatic range (red field), whereas the dashed lines show the melt composition. In both cases, crystallisation proceeds from high  $\text{V}_2\text{O}_3$ /light  $\delta^{51}\text{V}$  to low  $\text{V}_2\text{O}_3$ /heavy  $\delta^{51}\text{V}$ , with the regions of I-type and A-type denoted, corresponding to crystallisation under oxidising and reducing conditions, respectively. See section 5.2.



Figure 1

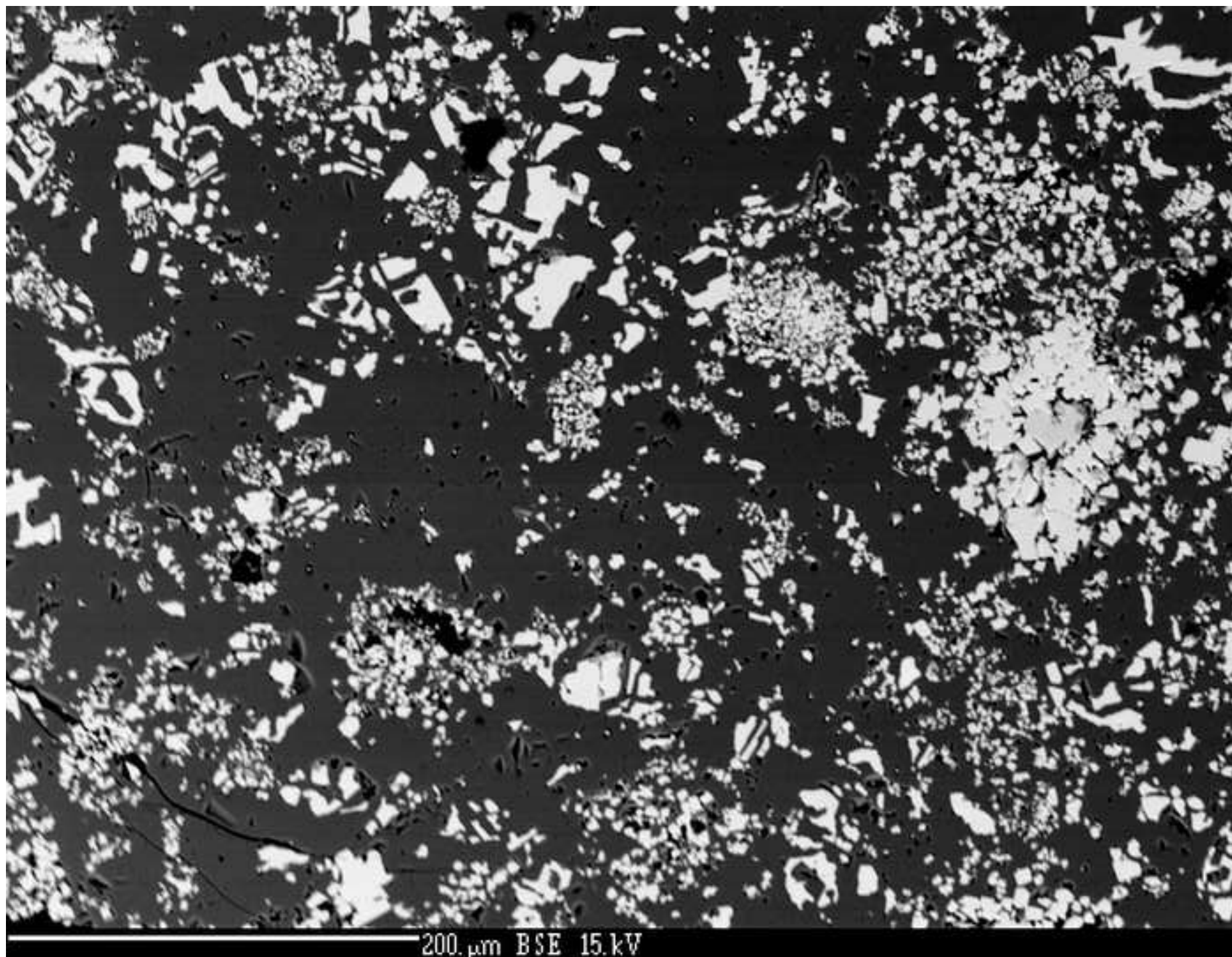


Figure 2

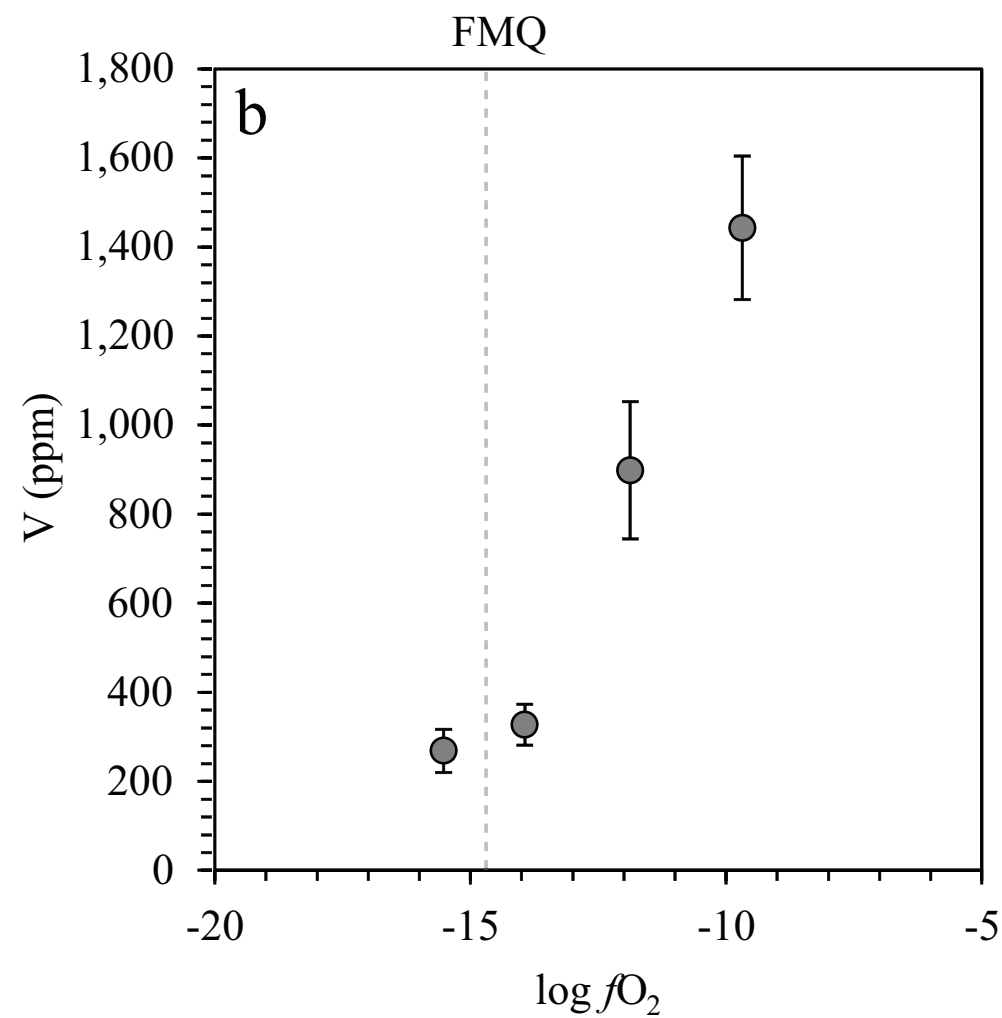
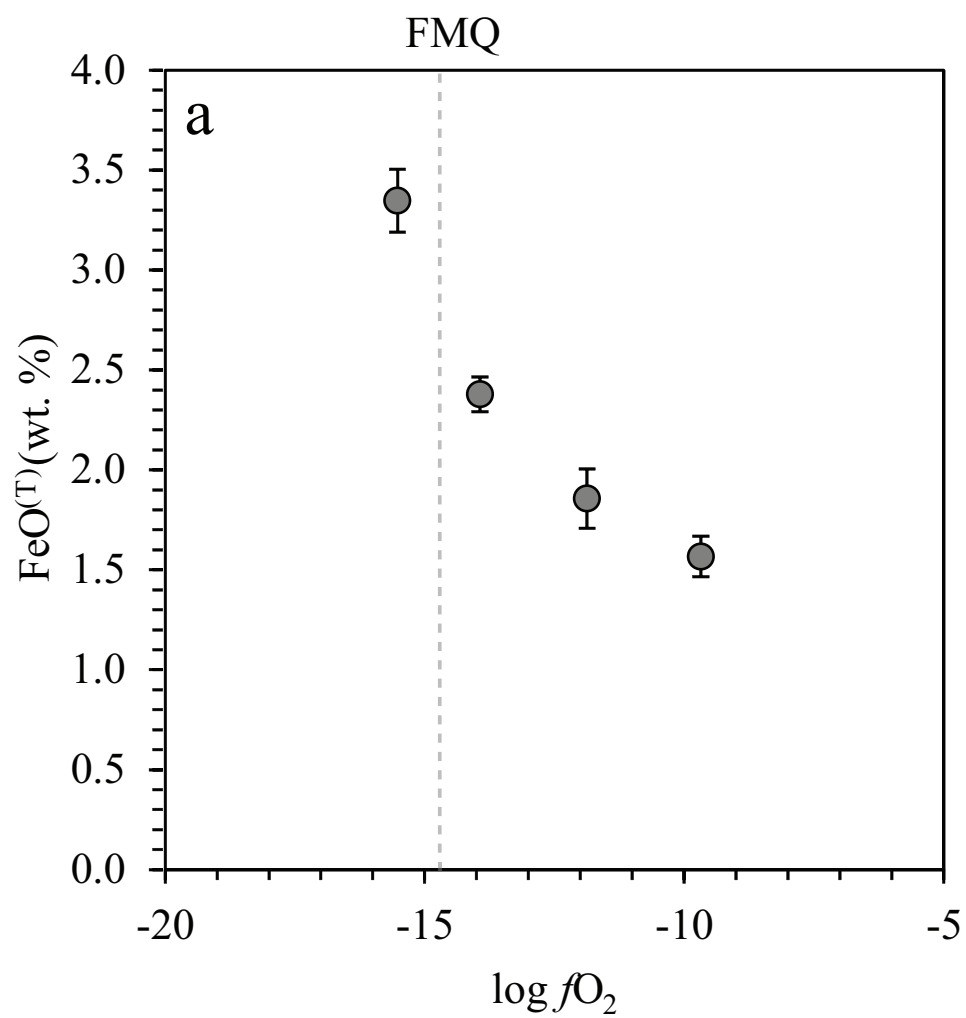


Figure 3

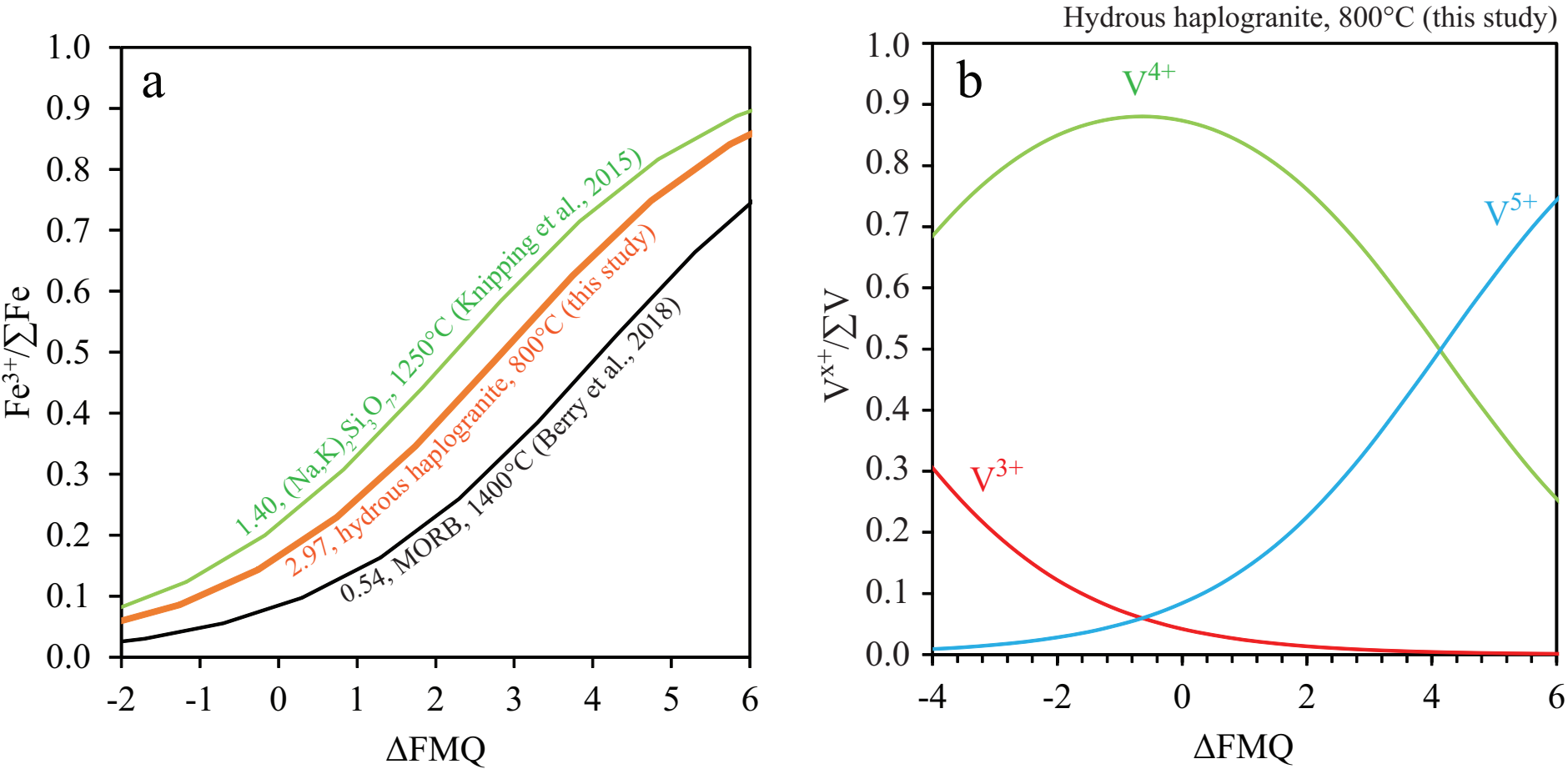


Figure 4

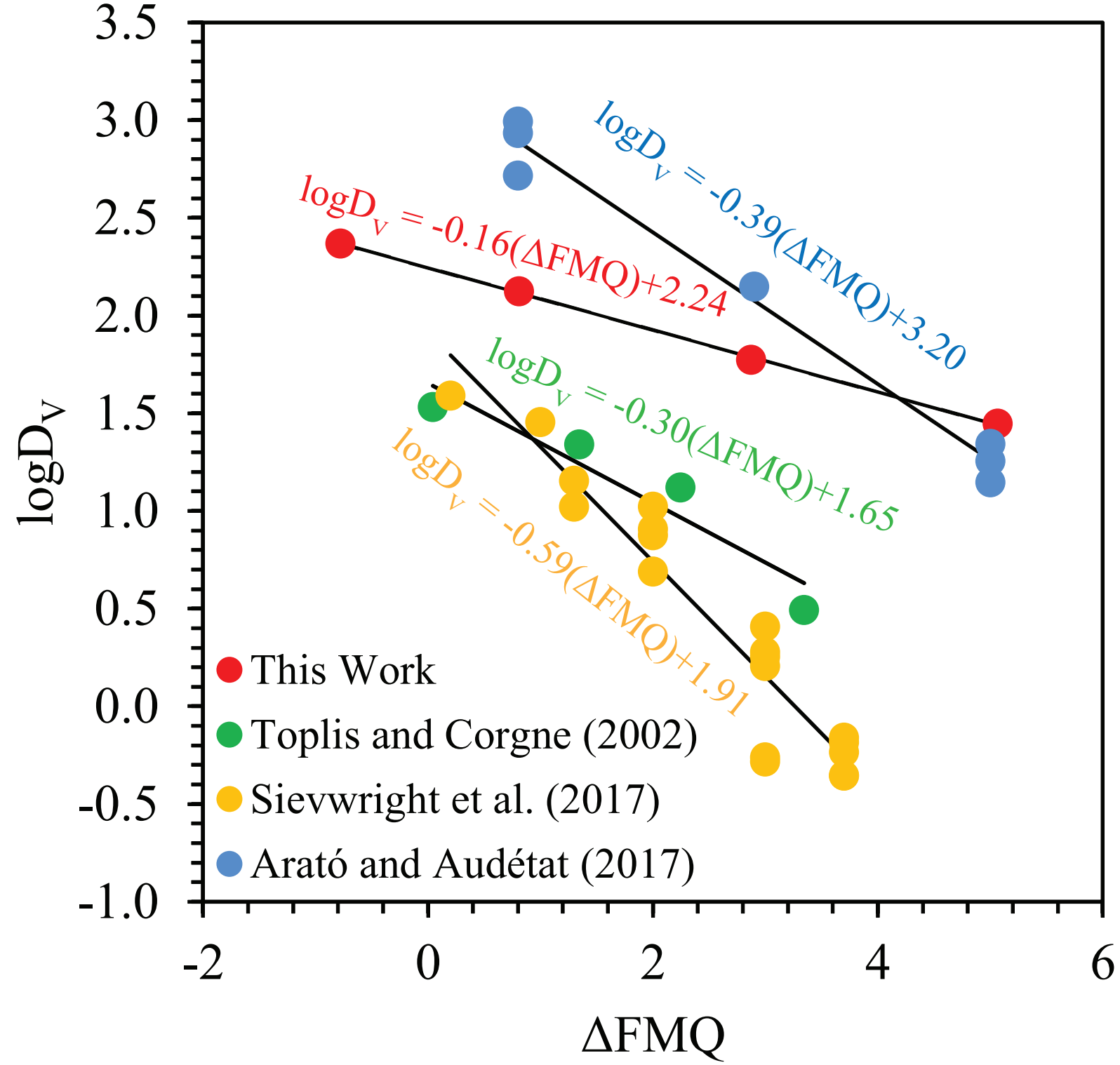
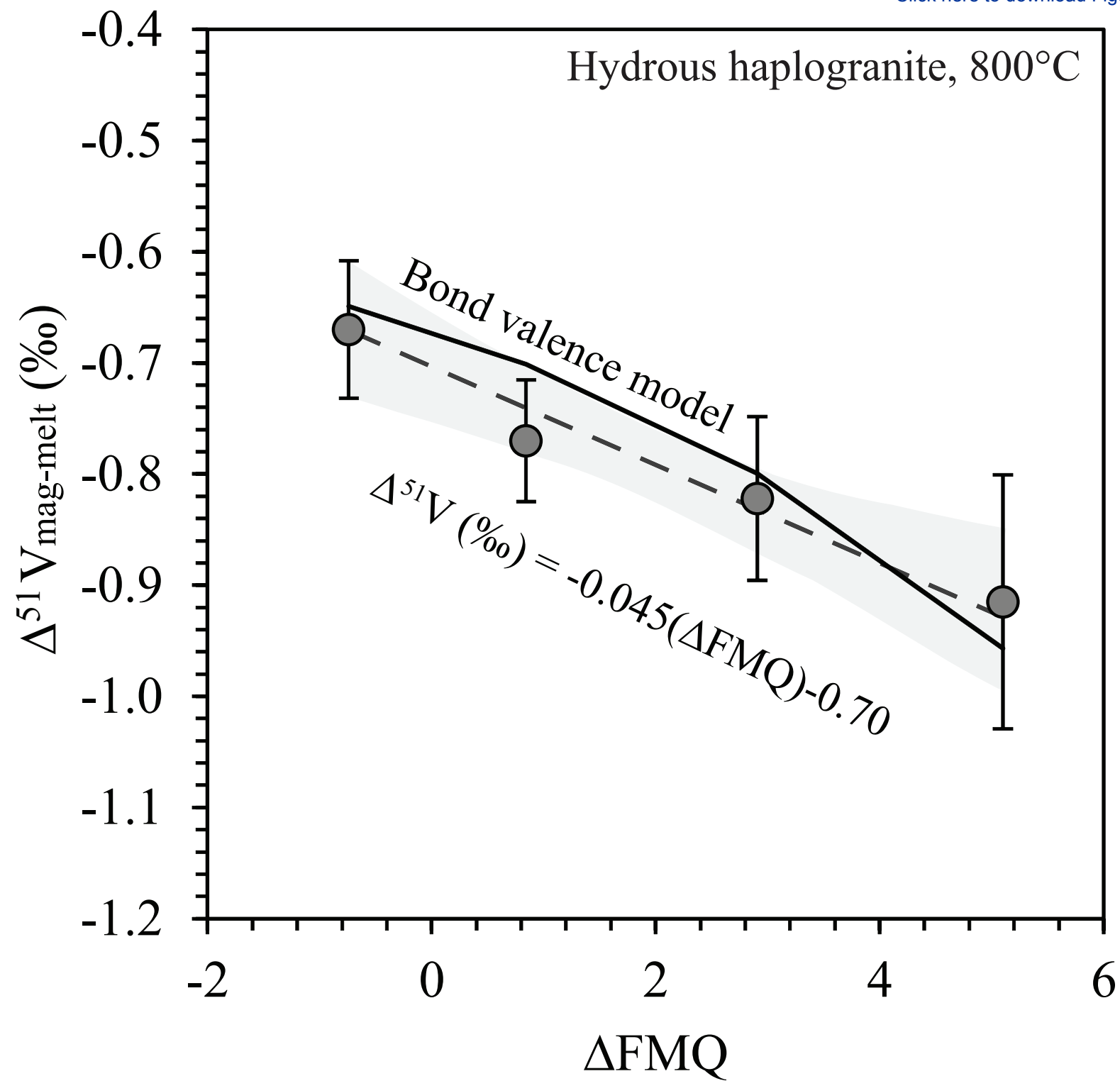
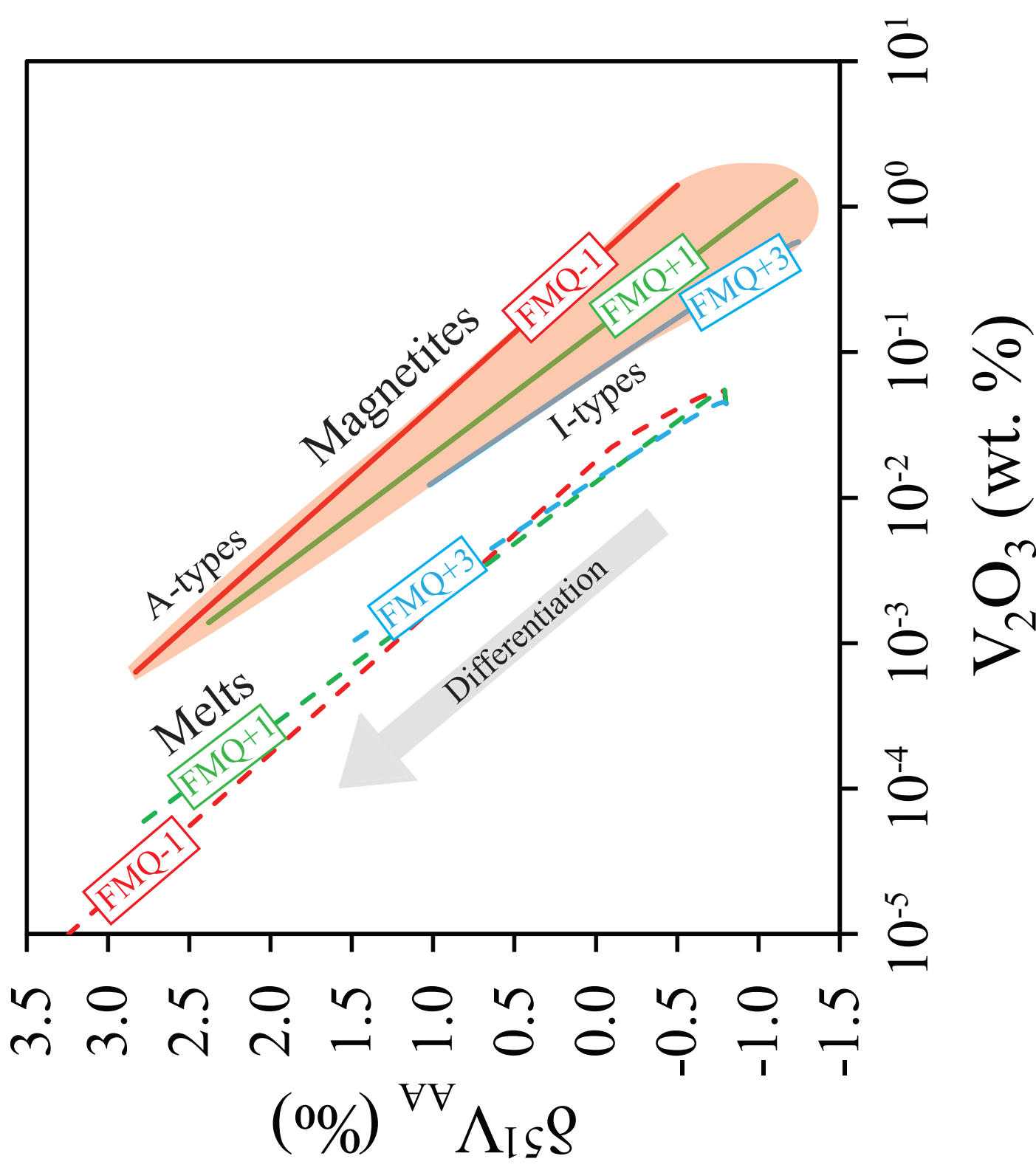


Figure 5





**Table 1.** Composition of experimental starting mix.

Component	Mass Fraction	Oxide (wt. %)						
		SiO <sub>2</sub>	Al <sub>2</sub> O <sub>3</sub>	Fe <sub>2</sub> O <sub>3</sub>	Na <sub>2</sub> O	K <sub>2</sub> O	V <sub>2</sub> O <sub>3</sub>	H <sub>2</sub> O
<i>Piston Cylinder</i>								
PS Haplogranite	0.460	77.64	12.90		4.73	4.74		
Magnetite	0.460			96.66				
Vanadium	0.039						100	
Water	0.041							0.043
<i>1 Atmosphere</i>								
Na-Fe-Silicate	0.980	37		38	23			
Vanadium	0.020						100	

**Table 2.** Experimental conditions and weights

Press	Name	Inner Capsule	Inner Capsule (g)	Mix (g)	H <sub>2</sub> O Inner (g)	Outer Ag (g)	Buffer Type	Buffer (g)	H <sub>2</sub> O Outer (g)	Temperature (°C)	Duration (h)	CO <sub>2</sub> (sccm)	CO (sccm)
V	D1542	<sup>75</sup> Ag- <sup>25</sup> Pd	0.2914	0.0686	0.0027	2.9989	HM	0.0547	0.0049	800	72	-	-
V	D1545	<sup>75</sup> Ag- <sup>25</sup> Pd	0.3069	0.0875	0.0040	2.9852	Co-CoO	0.0516	0.0084	800	72	-	-
A	C4449	<sup>75</sup> Ag- <sup>25</sup> Pd	0.2216	0.0547	0.0024	3.0045	NNO	0.1572	0.0311	800	336	-	-
V	D1555	<sup>75</sup> Ag- <sup>25</sup> Pd	0.2530	0.0637	0.0026	2.9788	Re-ReO <sub>2</sub>	0.0982	0.0058	800	168	-	-
C	FMQ-1	Ag	-	-	-	-	CO-CO <sub>2</sub>	-	-	800	163	98	5



**Table 3.** Cup configuration on Neptune Plus MC-ICP-MS

Cup	L3	L2	L1	C	H1	H2	H3
Resistor	10 <sup>11</sup>		10 <sup>11</sup>	10 <sup>10</sup>		10 <sup>11</sup>	10 <sup>11</sup>
Isotope	<sup>49</sup> Ti		<sup>50</sup> V	<sup>51</sup> V		<sup>52</sup> Cr	<sup>53</sup> Cr

**Table 4.** Compositions of experimental phases determined by electron microprobe.

Glasses	<i>n</i>	Oxide (wt. %)								Total
		Na <sub>2</sub> O	MgO	SiO <sub>2</sub>	Al <sub>2</sub> O <sub>3</sub>	FeO	K <sub>2</sub> O	CaO	V <sub>2</sub> O <sub>3</sub>	
<b>HM</b>	6	2.62	0.01	72.84	12.57	1.57	3.20	0.09	0.21	93.11
<b>±</b>		0.04	0.01	0.90	0.25	0.10	0.13	0.02	0.02	1.13
<b>Re-ReO<sub>2</sub></b>	6	2.58	0.01	71.36	12.94	1.86	3.31	0.09	0.13	92.30
<b>±</b>		0.07	0.02	0.74	0.56	0.15	0.11	0.02	0.02	0.32
<b>NNO</b>	8	3.35	0.04	68.04	13.77	2.38	2.80	0.12	0.05	90.55
<b>±</b>		0.23	0.01	0.49	0.22	0.09	0.09	0.02	0.01	0.65
<b>Co-CoO</b>	5	2.49	0.03	70.96	12.69	3.35	3.28	0.11	0.04	92.97
<b>±</b>		0.06	0.02	0.54	0.08	0.16	0.04	0.02	0.01	0.66
<b>FMQ-1</b>	5	17.68	0.04	49.04	0.17	26.38	0.06	0.25	2.67	96.29
<b>±</b>		0.08	0.02	0.20	0.02	0.25	0.02	0.03	0.03	0.48
<hr/>										
<b>Magnetite</b>										
<b>HM</b>	11		0.12	0.25	0.83	86.23			6.89	94.33
<b>±</b>			0.02	0.32	0.10	0.35			0.27	1.24
<b>Re-ReO<sub>2</sub></b>	8		0.10	0.12	1.02	83.71			7.83	92.78
<b>±</b>			0.03	0.03	0.14	1.04			1.06	0.08
<b>NNO</b>	7		0.10	0.06	0.60	82.14			8.14	91.03
<b>±</b>			0.05	0.07	0.16	0.69			0.65	0.88
<b>Co-CoO</b>	6		0.02	0.08	0.10	84.40			8.39	92.98
<b>±</b>			0.03	0.03	0.03	0.35			0.05	0.32
<b>FMQ-1</b>	6		0.01	0.09	0.00	91.87			0.33	92.31
<b>±</b>			0.01	0.02	0.02	0.62			0.10	0.65
<i>3 Cations/4 Oxygens</i>			<i>Mg<sup>2+</sup></i>	<i>Si<sup>4+</sup></i>	<i>Al<sup>3+</sup></i>	<i>Fe<sup>2+</sup></i>	<i>Fe<sup>3+</sup></i>		<i>V<sup>3+</sup></i>	<i>X<sub>Coul</sub></i>
<b>HM</b>	11		0.007	0.010	0.037	1.003	1.732		0.210	0.108
<b>Re-ReO<sub>2</sub></b>	8		0.006	0.005	0.046	0.999	1.705		0.240	0.123
<b>NNO</b>	7		0.005	0.002	0.027	0.997	1.719		0.249	0.127
<b>Co-CoO</b>	6		0.006	0.001	0.002	0.995	1.740		0.257	0.129
<b>FMQ-1</b>	6		0.001	0.004	0.000	1.003	1.983		0.010	0.005

**Table 5.** Vanadium stable isotope compositions of reference materials and standards.

	# dissolutions	# repetitions	$\delta^{51}\text{V}_{\text{AA}}$ (‰)	SD	2SE	Reference
V <sub>2</sub> O <sub>3</sub> (BDH)	2	3	-1.17	0.16	0.18	
BDH Solution	N/A	28	-1.13	0.06	0.03	
Column BDH	N/A	3	-1.22	0.12	0.16	
Column AA	N/A	3	-0.12	0.11	0.13	
<b>BCR2</b>	<b>1</b>	<b>2</b>	<b>-1.11</b>	<b>0.04</b>	<b>0.06</b>	<b>This Work</b>
BCR2			-0.95	0.08		Prytulak et al., 2011
BCR2			-0.78	0.04		Wu et al. (2016)
BCR2			-1.03	0.05		Schuth et al. (2017)
<b>BIR-1</b>	<b>3</b>	<b>7</b>	<b>-1.05</b>	<b>0.11</b>	<b>0.08</b>	<b>This Work</b>
BIR-1			-0.94	0.08		Prytulak et al., 2011
BIR-1			-0.92	0.05		Wu et al. (2016)
<b>PCC-1</b>	<b>1</b>	<b>2</b>	<b>-1.02</b>	<b>0.08</b>	<b>0.11</b>	<b>This Work</b>
PCC-1			-1.02	0.04		Prytulak et al., 2011

**Table 6.** Calculated bulk V content and isotope composition in the experiment and in the magnetite and glass solution fractions, their isotope composition, and the fractionation factor calculated after correcting for contamination.

Experiment	Bulk V <sub>2</sub> O <sub>3</sub> (wt. %)	± (SD)	Phase	V (ppm)	<i>f</i> <sub>mag</sub>	<i>f</i> <sub>gl</sub>	<i>n</i>	δ <sup>51</sup> V <sub>AA</sub> (‰)	± (SD)	δ <sup>51</sup> V <sub>AA,corr.</sub> (‰)	Bulk δ <sup>51</sup> V <sub>AA</sub> (‰)	Δ <sup>51</sup> V <sub>mag-gl</sub> (‰)	± (SD)
HM	3.60	0.31	Magnetite	28523			3	-1.48	0.07	-1.49	-1.46	<b>-0.92</b>	0.11
			Glass	3852	0.053		2	-1.16	0.09	-0.57			
Re-ReO <sub>2</sub>	3.98	0.10	Magnetite	29397			3	-1.45	0.06	-1.45	-1.43	<b>-0.82</b>	0.09
			Glass	1954	0.038		2	-1.08	0.07	-0.63			
NNO	3.41	0.16	Magnetite	34197			3	-1.79	0.06	-1.79	-1.73	<b>-0.77</b>	0.08
			Glass	327	0.004		2	-1.09	0.06	-1.02			
Co-CoO	4.22	0.24	Magnetite	25668			3	-1.35	0.06	-1.35	-1.33	<b>-0.67</b>	0.08
			Glass	520	0.014		1	-0.98	-	-0.68			
FMQ-1*	1.82	0.06	Magnetite	2890		0.04	1	-1.35	-	-1.51	-0.95	<b>-0.63</b>	0.09
			Glass	13545			2	-0.88	0.09	-0.88			

\* FMQ-1 is a 1 atm experiment

NB: Isotope compositions are quoted following correction for contamination (see *Correction for contamination and open-system behaviour of V in experiments*)



**Table 7.** Values of equilibrium constants and resulting  $\text{Fe}^{2+}/\text{Fe}^{3+}$  and  $\text{V}^{3+}/\text{V}^{4+}/\text{V}^{5+}$  ratios in the melt calculated by least-squares fit to the experimental partitioning data. Numbers in brackets refer to 1SD uncertainties. See *Partitioning and redox-dependence of Fe and V*.

	$\text{Log } K^*_{(9)}$	$\text{Log } K^*_{(10)}$	$\text{Log } K^*_{(15)}$	$\text{Log } K^*_{(17)}$	$\text{Log } K^*_{(18)}$	
<i>Global</i>	6.34(30)	2.97(8)	11.09(19)	5.04(12)	2.65(10)	
$\chi^2$	5.48			0.15		
	$\text{Fe}^{3+}/\sum \text{Fe}$		$\text{V}^{3+}/\sum \text{V}$	$\text{V}^{4+}/\sum \text{V}$	$\text{V}^{5+}/\sum \text{V}$	$\text{V}^{\text{av}}/\sum \text{V}$
<i>Co-CoO</i>	0.12(2)		0.06(2)	0.88(4)	0.06(2)	4.00(1)
<i>Ni-NiO</i>	0.24(3)		0.02(1)	0.85(5)	0.13(3)	4.11(3)
<i>Re-ReO<sub>2</sub></i>	0.52(4)		0.01(0)	0.66(7)	0.34(5)	4.33(5)
<i>HM</i>	0.80(2)		0.00(0)	0.35(9)	0.65(9)	4.65(10)

**Table 8.** Parameters for calculating the isotope fractionation from the bond valence model. See *Controls on V isotope fractionation*. z = valence, v = co-ordination, s = bond valence, r = bond length, K<sub>f</sub> = force constant.

Experiment	Phase	z <sub>v</sub>	v <sub>v</sub>	s <sub>v</sub>	s <sub>o</sub>	r <sub>v,o</sub> (m)	K <sub>f</sub> (N/m)	± (SD)
HM	Magnetite	3.00	6	0.50	0.50	2.00×10 <sup>-10</sup>	281	56
	Melt	4.65	4.5	1.03	0.80	1.79×10 <sup>-10</sup>	890	178
Re-ReO <sub>2</sub>	Magnetite	3.00	6	0.50	0.50	2.00×10 <sup>-10</sup>	281	56
	Melt	4.33	4.5	0.96	0.80	1.83×10 <sup>-10</sup>	815	163
NNO	Magnetite	3.00	6	0.50	0.50	2.00×10 <sup>-10</sup>	281	56
	Melt	4.11	4.5	0.91	0.80	1.85×10 <sup>-10</sup>	749	150
Co-CoO	Magnetite	3.00	6	0.50	0.50	2.00×10 <sup>-10</sup>	281	56
	Melt	4.00	4.5	0.89	0.80	1.87×10 <sup>-10</sup>	715	143